Crystal structure analysis of the outer membrane factors of multidrug efflux pumps from *Pseudomonas aeruginosa*

(緑膿菌由来多剤排出ポンプの外膜因子の結晶構造解析)

A doctoral thesis

By

Ryo Yonehara

Submitted to the Graduate School of Science

Osaka University

Japan

February, 2016

Acknowledgement

This study has been carried out under the direction of Professor Atsushi Nakagawa of Institute for Protein Research, Osaka University. I would like to thank him for his incessant guidance and encouragement throughout this study.

I would like to express my deep appreciation for Assistant Professor Eiki Yamashita of Institute for Protein Research, Osaka University for prominent guidance for this study.

I want to thank Professor Junichi Takagi and Professor Genji Kurisu of Institute for Protein Research, Osaka University for their helpful suggestions and comments.

I also thank all members of Laboratory of Supramolecular Crystallography in Institute for Protein Research, Osaka University for their kindness and helpful suggestions.

Finally, I really thank my parents for their understanding and supports.

Ryo Yonehara

February 2016

Table of contents

Abbreviation

AcrA	Acridine resistance protein A
AcrB	Acridine resistance protein B
BL	beam line
CCP4	Collaborative Computational Project, Number 4
DNase I	Deoxyribonuclease I
EM	Electron microscopy
EMDB	Electron Microscopy Data Bank
kDa	kilo-Dalton
MexA	Multidrug efflux component A
MexB	Multidrug efflux component B
MexC	Multidrug efflux component C
MexD	Multidrug efflux component D
MexE	Multidrug efflux component E
MexF	Multidrug efflux component F
MFP	Membrane fusion protein
MFS	Major facilitator superfamily
MPD	2-methyl-2,4-pentanediol
MR	Molecular replacement
OG	*n*-octyl-β-D-glucopyranoside
OprJ	Outer membrane protein J
OprM	Outer membrane protein M
OprN	Outer membrane protein N
PCR	Polymerase chain reaction
PDB	Protein Data Bank

PEG	Polyethylene glycol
rmsd	root mean square deviation
RND	Resistance nodulation cell division
SDS-PAGE	Sodium dodecyl sulfate-polyacrylamide gel electrophoresis
SPring-8	Super Photon Ring-8

Chapter 1
Introduction

1.1 *Pseudomonas aeruginosa* and multidrug resistance

Pseudomonas aeruginosa is a Gram-negative aerobic and rod-shaped indigenous bacterium in a natural environment. *P. aeruginosa* shows low pathogenicity to healthy individuals, whereas infection to immunocompromised hospital patients often threatens their life. This bacterium is one of causative microorganisms causing opportunistic and nosocomial infection. It shows natural intrinsic resistance to structurally and functionally dissimilar antibiotics, including β-lactams, fluoroquinolones, tetracycline, chloramphenicol, erythromycin, and novobiocin (Gotoh, N. *et al.* 1998; Maseda, H. *et al.* 2000). The natural intrinsic multidrug resistance is mainly caused by expression of tripartite efflux pumps and low permeability of its outer membrane (Morshed, S. R. *et al.* 1995; Li, X. Z. *et al.* 1995; Nakae, T. 1995; Nikaido, H. 1994).

1.2 MexAB-OprM

Tripartite efflux pump consists of a resistance nodulation cell division (RND) transporter, a membrane fusion protein (MFP), and an outer membrane factor (OMF) (Schweizer, H. P. 2003) (Figure 1.1). In *P. aeruginosa*, MexAB-OprM is responsible for intrinsic multidrug resistance (Morshed, S. R. *et al.* 1995; Li, X. Z. *et al.* 1995).

MexAB-OprM consists of three components, MexA, MexB, and OprM, which belong to MFP, RND, and OMF, respectively. MexB recognizes and transports antibiotics to OMF through structural change using energy stored in the proton gradient across the inner membrane (Lei, Y. *et al.* 1991; Guan, L. *et al.* 2001). The crystal structures of MexB were determined at 3.0 Å and 2.7 Å resolution (Figure 1.2A) (Sennhauser, G. *et al.* 2009; Nakashima, R. *et al.* 2013). Furthermore, the crystal structures of AcrB, which

is an *Escherichia coli* ortholog of MexB, were also determined with antibiotics at 1.9 Å and 2.25 Å resolution (Figure 1.2B) (Eicher, T. *et al.* 2012). The crystal structures of MexB and AcrB revealed that RND transporter consists of three domains: docking, porters, and transmembrane domains (Figure 1.2). RND transporter is a homotrimer, and it is postulated that each monomer shifts conformational states (access, bind, and extrusion, or loose, tight, and open) by using the proton motive force (Figure 1.2C) (Murakami, S. *et al.* 2006; Seeger, M. A. *et al.* 2006; Sennhauser, G. *et al.* 2009). In AcrB, the high resolution atomic structures revealed that RND transporter has two antibiotic binding sites (access and deep binding pockets), and that the switch loop

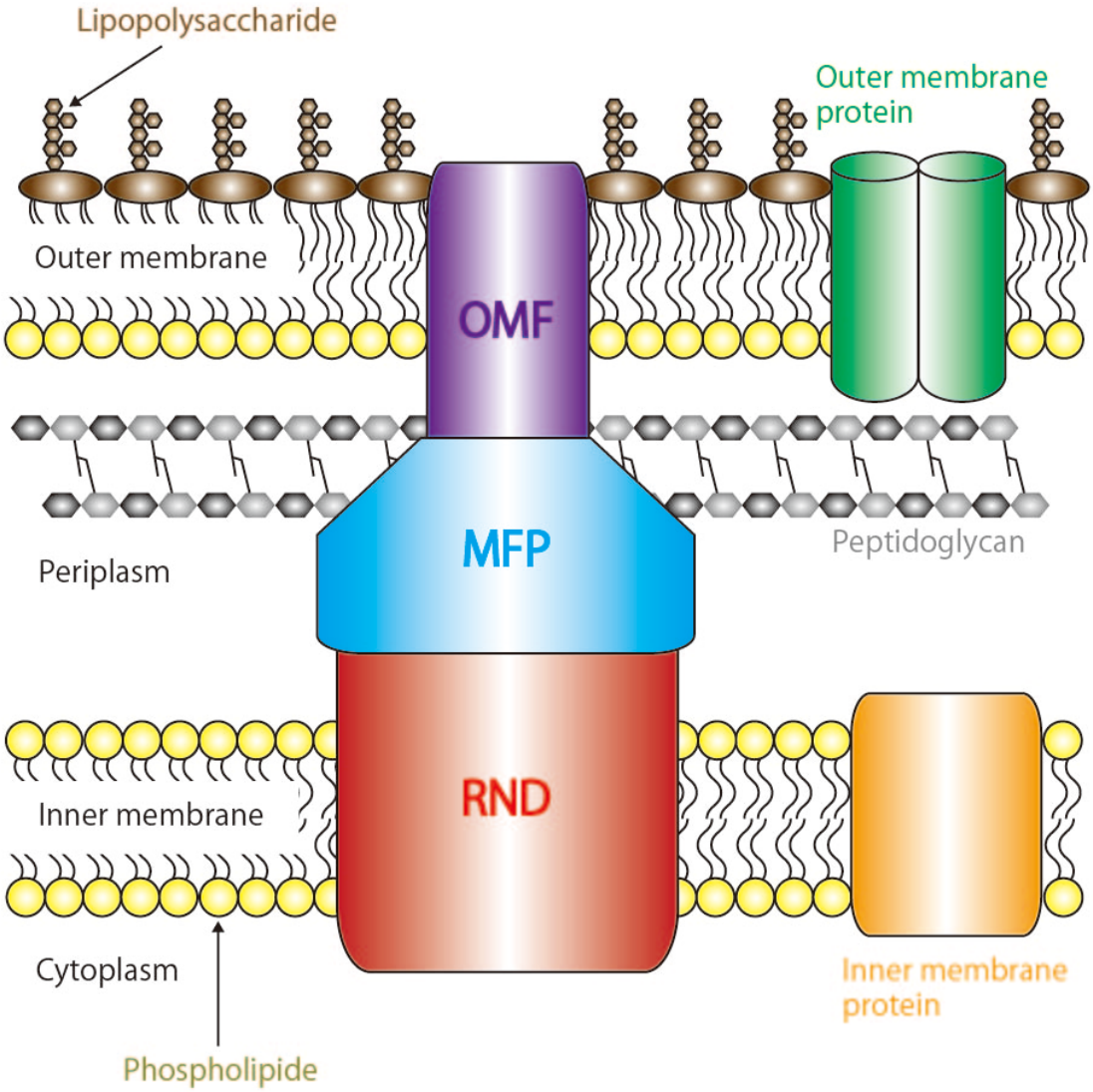

Figure 1.1 Schematic representation of tripartite efflux pump

locates in the middle of these binding sites (Figure 1.2C and 1.2D). Antibiotics binding at the access binding pocket are transported sequentially to the deep binding pocket and to OMF during the structural conformational change. Since MexB has high amino acid sequence identity to AcrB (69.9%) and overall structural similarity, the extruding mechanism of MexB is thought to be same of AcrB.

OprM forms a channel to facilitate the extrusion of antibiotics through the outer membrane (Nakajima, A. *et al.* 2000). The crystal structures of OprM were determined at 2.56 Å and 2.4 Å resolution (Figure 1.3A) (Akama, H. *et al.* 2004; Phan, G. *et al.* 2010). Moreover, the crystal structure of TolC, which is an *E. coli* ortholog of OprM, was also reported (Fiugre 1.3B), and showed that antibiotic entrance to its internal cavity was closed (Koronakis, V. *et al.* 2000). Based on the X-ray crystallography of TolC mutants, an opening mechanism of the gate was proposed (Koronakis, V. *et al.* 2000; Bavro, V. N. *et al*. 2008; Pei, X. Y. *et al.* 2011). The mechanism is postulated that inner coiled-coil helices (H7/H8) of TolC undergo an iris-like movement to open the gate, that outer coiled-coil helices (H3/H4) support the rearrangement of the inner coiled-coil helices. Overall structures of OprM and TolC are similar, but amino acid sequence similarity between OprM and TolC is low (27.5%). Thus, in OprM, the structural rearrangements of the inner and outer coiled-coil helices to open the gate are unclear.

MexA is anchored to the inner membrane via fatty acids attached to the N-terminal cysteine (Yoneyama, H. *et al.* 2000). MexA is an essential component of the tripartite efflux pump, and deletion of MexA showed hypersusceptible to a large number of antibiotics (Yoneyama, H. *et al*. 1997). The crystal structures of MexA were determined at 2.4 Å and 3.2 Å resolution (Figure 1.4A) (Akama, H. *et al*. 2000; Symmons, M. F. *et al.* 2009). Furthermore, the crystal structure of AcrA, which is an *E. coli* ortholog of MexA, was also determined (Figure 1.4B) (Mikolosko, J. *et al.* 2006). In the crystal

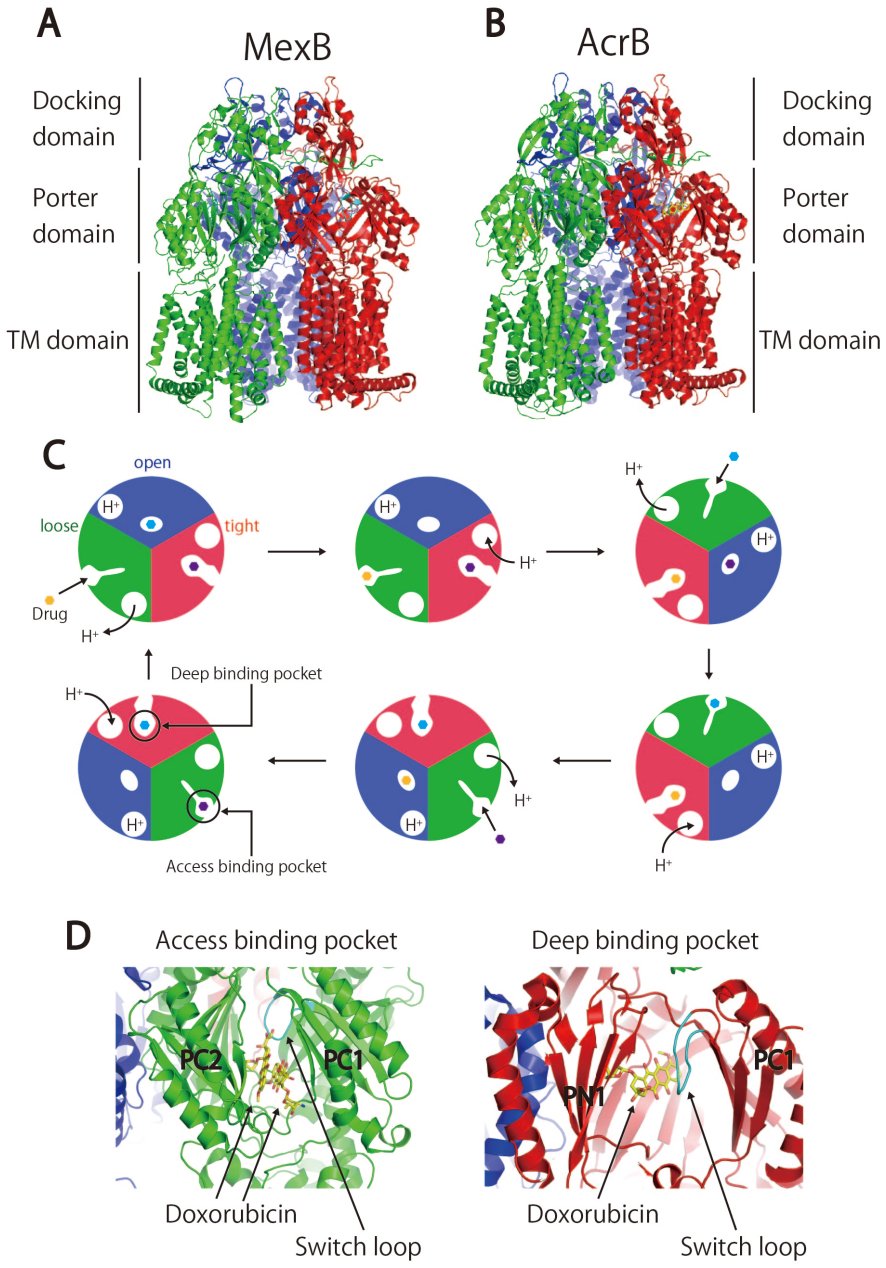

Figure 1.2 Crystal structures of MexB and AcrB

(A, B) Crystal structures of MexB (PDB ID: 2V50) (A) and AcrB (PDB ID: 4DX7) (B) are shown as ribbon diagrams. Loose, tight, open protomers and switch loop are colored in green, red, blue, and cyan respectively. (C) Schematic representation of porter domains showing each conformational state. (D) Close-up views of access and deep binding pockets of AcrB. Doxorubicin is shown as a stick model. Carbon, nitrogen, and oxygen atoms are colored in yellow, blue, and red, respectively.

structure of AcrA, MP domain was disordered, but it is assumed that its structure is similar to that of MexA due to high identity in amino acid sequence between each other (59.7%). The crystal structures of MexA and AcrA revealed that MFP consists of four domains: α-hairpin, lipoyl, β-barrel, and MP domains (Figure 1.4). Among these domains, α-hairpin domain is important for interaction with OMF, and determines binding specificity between OMF and MFP (Eda, S. *et al.* 2006). In the tripartite efflux pump, MFP interacts with the docking and porter domains of RND transporter, and α-hairpin domain of MFP forms a cylinder structure and interacts with the periplasmic end of α-barrel domain of OMF (Figure 1.5) (Du, D. *et al*. 2014). However, residues involved in the interaction between OMF and MFP has yet been identified due to insufficiency of resolution.

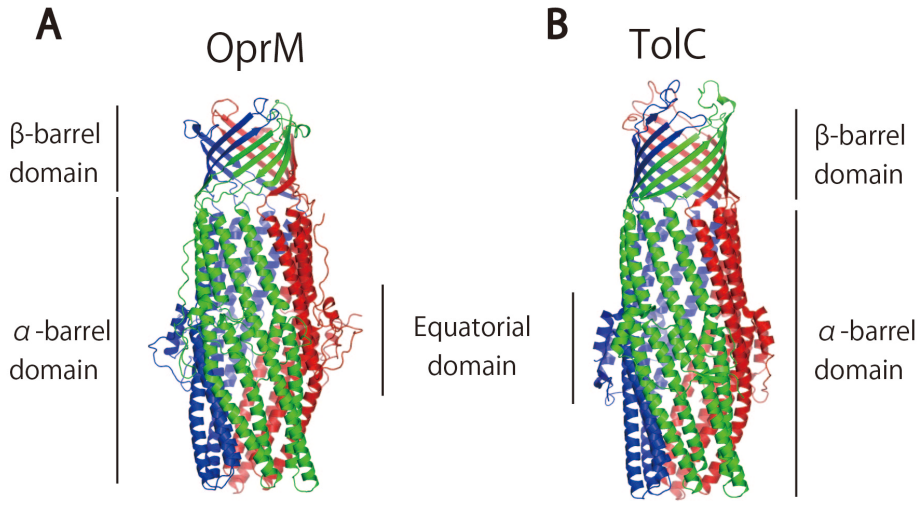

Figure 1.3 Crystal structures of OprM and TolC

(A, B) Crystal structures of OprM (PDB ID: 1WP1) (A) and TolC (PDB ID: 1EK9) (B) are shown as ribbon diagrams. Each protomer is colored in green, blue, and red respectively.

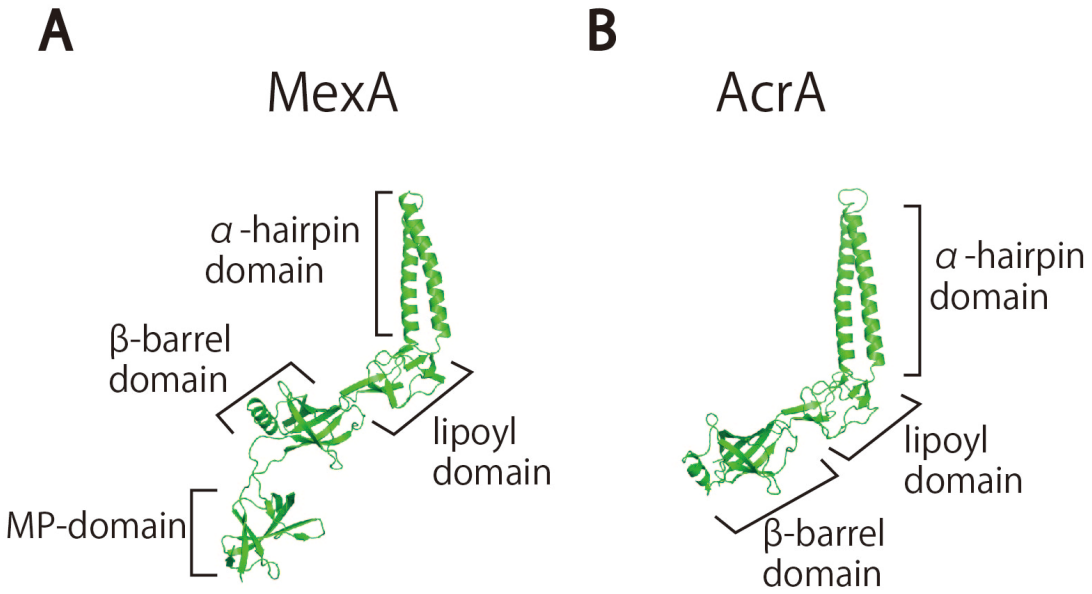

Figure 1.4 Crystal structures of MexA and AcrA

(A, B) Crystal structures of MexA (PDB ID: 2V4D) (A) and AcrA (PDB ID: 2F1M) (B) are shown as ribbon diagrams.

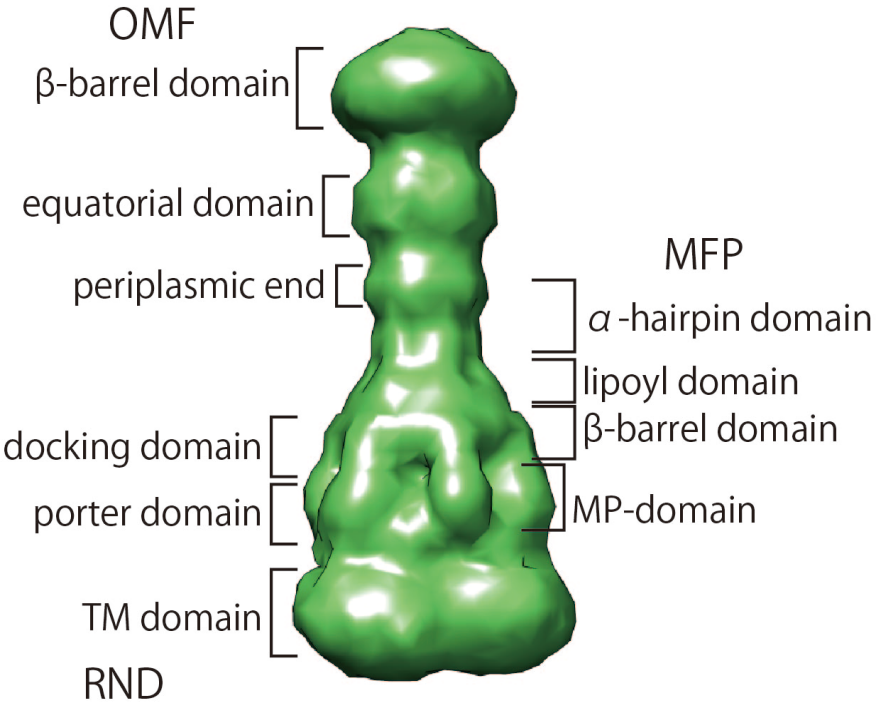

Figure 1.5 model of tripartite efflux pump

EM map (EMDB accession code: 5915) was generated by Chimera (Pettersen, E. F. *et al*. 2004).

1.3 Other tripartite efflux pumps in *P. aeruginosa*

In addition to MexAB-OprM, many tripartite efflux pumps have been identified: MexCD-OprJ (Gotoh, N. *et al.* 1998; Poole, K. *et al.* 1996), MexEF-OprN (Maseda, H. *et al.* 2000; Köhler, T. *et al.* 1997), MexXY-OprM (Mine, T. *et al.* 1999; Wadman, S. W. *et al.* 1999), MexHI-OpmD (Sekiya, H. *et al.* 2003), MexPQ-OpmE (Mima, T. *et al.* 2005), MexJK-OprM (Chuanchuen, R. *et al.* 2002), MexMN-OprM (Mima, T. *et al.* 2005), MexVW-OprM (Li, Y. *et al.* 2003), MuxABC-OpmB (Mima, T. *et al.* 2009), TriABC-OpmH (Mima, T. *et al.* 2007), and CzcBA-CzcC (Hassan, M. T. *et al.* 1999) (Table 1). Among these tripartite efflux pumps, MexAB-OprM, MexCD-OprJ, MexEF-OprJ, and MexXY-OprM are important for multidrug resistance of *P. aeruginosa*. Overexpression of either MexAB-OprM, MexCD-OprJ, MexEF-OprN or MexXY-OprM drastically decreases susceptibility to antibiotics (Morshed, S. R. *et al.* 1995; Gotoh, N. *et al*. 1998; Maseda, H. *et al.* 2000, Mine, T. *et al.* 1999). Main antibiotics transported by each tripartite efflux pump are different: β-lactams in MexAB-OprM, fluoroquinolones in MexCD-OprJ, chloramphenicol in MexEF-OprN, and aminoglycosides in MexXY-OprM. Mutants overexpressing either MexAB-OprM, MexCD-OprJ or MexEF-OprN are known as *nalB* (Saito, K. *et al.* 1999), *nfxB* (Shiba, T. *et al*. 1995; Poole, K. *et al.* 1996), *nfxC* (Fukuda, H. *et al.* 1990), respectively. Expression of MexAB-OprM, MexCD-OprJ, and MexXY are negatively regulated by a product of the *mexR* (Saito, K. *et al.* 1999), *nfxB* (Shiba, T. *et al.* 1995), and *mexZ* (Matsuo, Y. *et al.* 2004) genes, respectively. In contrast, the expression of MexEF-OprN is positively regulated by the *mexT* (Maseda, H. *et al.* 2000) gene.

P. aeruginosa has a large number of tripartite efflux pumps than other multidrug resistant Gram-negative bacteria, such as *E. coli* and *Acinetobacter baumannii* (Table 1). This is a unique feature for *P. aeruginosa*. In *E. coli*, TolC is only OMF except for CusC and has an ability to form functional tripartite efflux pumps with a number of

combinations of RND and MFP. In *P. aeruginosa*, OprM can form functional tripartite efflux pumps with MexXY, MexJK, MexMN, and MexVW, however, most of OMFs have a specific MFP-RND transporter.

Table 1 Tripartite efflux pumps in Gram-negative bacteria

Organism	Efflux components			Antibiotics[a]
	MFP	RND	OMF	
P. aeruginosa	MexA	MexB	OprM	AC, AZT, CP, EB, EM, NFLX, NV, TC, SDS, TPP
	MexC	MexD	OprJ	AC, CP, EB, EM, NFLX, NV, TC, SDS, TPP
	MexE	MexF	OprN	CP, NFLX
	MexX	MexY	OprM	EM, KM, NFLX, TC
	MexH	MexI	OpmD	AC, EB, NFLX
	MexP	MexQ	OpmE	EM
	MexJ	MexK	OprM	EM, TC, TS
	MexM	MexN	OprM	CP
	MexV	MexW	OprM	AC, CP, EB, EM, NFLX, TC
	MuxA	MuxB, MuxC	OpmB	AZT, NV, EM
	TriA, TriB	TriC	OpmH	TS
	CzcB	CzcA	CzcC	Cd^{2+}, Zn^{2+}

(*Table 1 continued*)

(Table 1 continued)

E. coli	AcrA	AcrB	TolC	AC, CP, EB, EM, NA, NFLX, NV, SDS, TC, TPP
	AcrA	AcrD	TolC	KM, NV, SDS
	AcrE	AcrF	TolC	AC, EB, SDS
	MdtA	MdtB, MdtC	TolC	FOM, NA, NFLX, NV, SDS
	MdtE	MdtF	TolC	EB, SDS, TPP
	CusB	CusA	CusC	Cu^+, Ag^+
A. baumannii	AdeA	AdeB	AdeC	CP, EM, NFLX, NV, TC
	AdeI	AdeJ	AdeK	AZT, CP, EM, NFLX, TC
	AdeF	AdeG	AdeH	CP, NFLX, TC

[a]AC, acriflavine; AZT, aztreonam; CP, chloramphenicol; EB, ethidium bromide; EM, erythromycin; FOM, fosfomycin; KM, kanamycin; NA, nalidixic acid; NFLX, norfloxacin; NV, novobiocin; TC, tetracycline; TS, triclosan; SDS, sodium dodecyl sulphate; TPP, tetraphenyl phosphonium

1.4 OMFs in *P. aeruginosa*

OprM, OprJ and OprN are the main OMFs in tripartite efflux pumps of *P. aeruginosa* and are essential components for MexAB, MexCD, and MexEF, respectively. *P. aeguginosa* mutants expressing only RND and MFP are hypersusceptibility to a large number of antibiotics (Yoneyama, H. *et al.* 1997; Gotoh, N. *et al.* 1998; Yoneyama, H. *et al.* 1998; Maseda, H. *et al*. 2000). However, a particular combination of OMF, RND, and MFP is not strictly required when the tripartite efflux pumps extrude antibiotics from the bacterial cell into the extracellular space (Table 2). For example, OprM can form a hetero-functional tripartite efflux pump with MexCD, MexEF, and MexJK as well as with MexAB (Gotoh, N. *et al.* 1998; Maseda, H. *et al.* 2000; Chuanchuen, R. *et al.* 2002). OprJ can also form a hetero-functional tripartite efflux pump with MexAB (Yoneyama, H. *et al.* 1998), whereas OprN cannot (Maseda, H. *et al.* 2000).

P. aeruginosa has other OMFs in addition to OprM, OprJ, and OprN: OpmB, OpmD, OpmE, and OpmH. Among these OMFs, OpmB can also form a hetero-functional tripartite efflux pump with MexAB and MexCD, but OpmD and OpmE cannot (Murata, T. *et al.* 2002) (Table 2). OpmH function with TriABC and MexJK (Chuanchuen, R. *et al.* 2005; Mima, T. *et al.* 2007), but does not form an operon. OpmH shows low amino acid sequence similarities among other OMFs, and specializes in extrusion of triclosan (Chuanchuen, R. *et al.* 2005).

The amino acid sequence alignment between OprM, OprN, and OprJ shows the similarities between OprN and OprM, and between OprJ and OprM are 44.7% and 59.1%, respectively (Table 3 and Figure 1.6). Pro86, Pro265, Pro273, Pro298, Gly199, Gly407, and N-terminal cysteine of OprM are conserved in OprN and OprJ. These proline residues determine staring points of secondary structures denoted as S1, H5, H6 and S3, respectively. Gly199 and Gly407 locate at a periplasmic tip of the α-barrel domain, and a susceptibility test showed that the G199A or G407A mutant have a

detrimental effect on MexAB-OprM function (Nehme, D. *et al.* 2007). The N-terminal cysteine is important for anchoring the outer membrane (Nakajima, A. *et al.* 2000). Furthermore, ELDLFGR and LGGGW motif of OprM are also conserved in OprN and OprJ. The deletions of these motifs affect stability and activity of OprM (Li, X. Z. *et al.* 2001; Bai, J. *et al.* 2014).

Table 2 Susceptibility tests for hetero tripartite efflux pumps

	MexAB	MexCD	MexEF	MexJK	MuxABC	MexGH	MexPQ	TriABC
OprM	++[a]	+	+	+	−	ND	ND	ND
OprJ	+[b]	++	ND	-	ND	ND	ND	ND
OprN	−[c]	ND[d]	++	-	ND	ND	ND	ND
OpmB	+	+	ND	ND	++	ND	ND	ND
OpmD	−	−	ND	ND	ND	++	ND	ND
OpmE	−	−	ND	ND	ND	ND	++	ND
OpmH	ND	ND	ND	+	ND	ND	ND	+

++[a], +[b], −[c], and ND[d] indicate operon, functional, non-functional combination, and not determination, respectively.

Table 3 Similarities (%) of amino acid sequence among OMFs

	OprM	OprJ	OprN	OpmB	OpmD	OpmE	OpmH
OprM							
OprJ	59.1						
OprN	44.7	46.4					
OpmB	44.7	44.0	40.6				
OpmD	41.9	43.4	53.8	37.1			
OpmE	42.7	44.7	49.2	48.6	48.6		
OpmH	29.7	26.5	22.6	22.6	26.5	27.3	

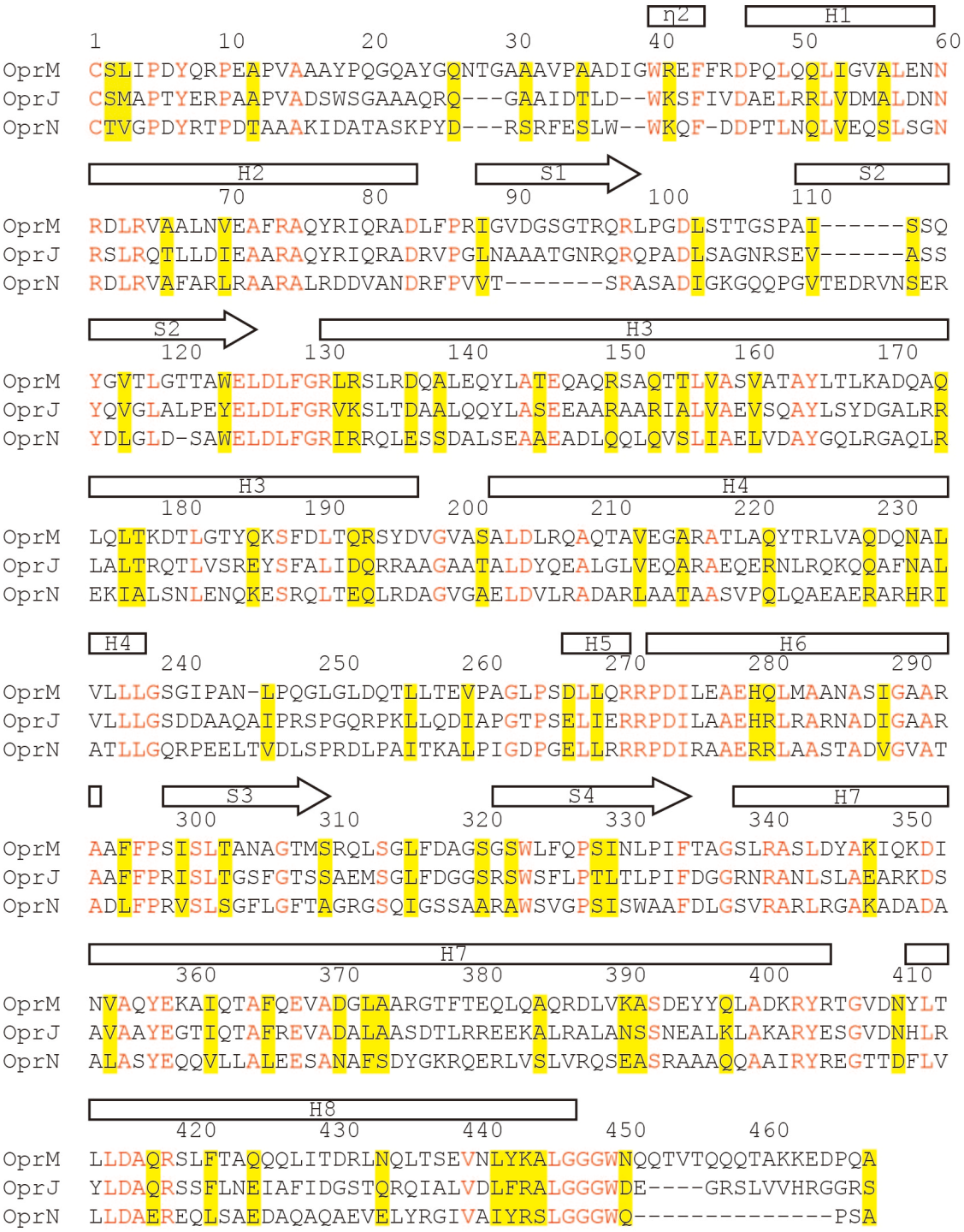

Figure 1.6 Sequence alignments of OprM, OprJ, and OprN

Conserved residues are colored in red and highly similar residues are shaded as yellow. The secondary structure of OprM is indicated above the alignment as a rectangle (α-helix) and an arrow (β-strand).

1.5 Purpose of this study

In addition to the crystal structures of OprM (Akama, H. *et al.* 2004; Phan, G. *et al.* 2010) and TolC (Koronakis, V. *et al.* 2000), those of other OMF have been reported: CmeC from *Campylobacter jejuni* (Su, C. C. *et al*. 2014), MtrE from *Neisseria gonorrhoeae* (Lei, H. T. *et al*. 2014), and VceC from *Vibrio cholerae* (Federici, L. *et al*. 2005). Among these OMFs, VceC forms the tripartite efflux pump with VceA and VceB, which belong to MFP and a major facilitator superfamily (MFS), respectively (Colmer, J. A. *et al.* 1998). Although the inner membrane component differs between VceC and ohter OMFs, the overall crystal structures were similar to each other, and revealed that OMF consists of conserved three domains: α-barrel, β-barrel, and equatorial domains (Figure 1.3). Based on this result and the amino acid sequence alignment between OprN, OprJ, and OprM, it is considered that the overall structures of OprN and OprJ are similar to that of OprM. However, in light of the high similarity in amino acid sequence between OprN, OprJ, and OprM (Table 3), it is difficult to explain the specific recognition of *P. aeruginosa* OMF at hetero-functional tripartite efflux pumps. Moreover, the structural character causing the selectivity of OprM for a number of MFP-RND transporters remain to be fully elucidated due to its crystal structure alone. Therefore, additional structural information of *P. aeruginosa* OMFs is necessary for elucidate the basis of specific recognition and selectivity for MFP-RND transporter. In this study, to understand the structural character of *P. aeruginosa* OMFs, we determined the crystal structures of OprN and OprJ.

Chapter 2
Material and Method

2.1 Cloning and expression

The *oprN* and *oprJ* genes were amplified by PCR from the *P*. *aeruginosa* the genomic DNA. All PCR primers are listed in Table 4. PCR products were ligated to the cloning vector pGEM-T easy (Promega), and were confirmed by DNA sequencing. After digesting each plasmid with the restriction enzymes *Nde*I and *Bam*HI, the fragments were extracted from an agarose gel and ligated to the modified expression vector pET21b+ (Novagen), which has a *Bam*HI site followed by a hexa-histidene tag.

OprN and OprJ were expressed in *E. coli* strain C43(DE3). The cells were cultured in 2xYT medium containing 50 μg/ml ampicillin at 310 K. When an optical density at 590 nm reached 0.6, the cultures were cooled down to 299 K and treated with 0.1 mM isopropyl-β-D-1-thiogalactopyranoside to induce *oprN* or *oprJ* expression. Following induction, cells were cultured for about 3 h. Next, cells were collected by centrifugation.

Table 4 Primer list

Primer name	Primer sequence
OprN_forward	CATATGATTCACGCGCAGTCGATCCGGAGCGGGCTCGC
OprN_reverse	GGATCCGGCGCTGGGTTGCCAGCCACCGCCGAGG
OprJ_forward	CATATGCGCAAACCTGCTTTCGGCGTATCGGCGCTGC
OprJ_reverse	GGATCCACTCCTGCCGCCTCGATGTACCACCAGGCTCC

2.2 Purification

The pellets were resuspended in 50 mM sodium phosphate (pH7.4), 100 mM NaCl, 2 mM $MgCl_2$, and 10 μg/ml DNase I, and disrupted using a high pressure homogenizer (APV 2000, SPX) at 800 psi. After unbroken cells were removed by centrifugation at 10,000*g* for 10 min, membrane fractions were collected by ultracentrifugation at 235,000*g* for 30 min and washed with 50 mM sodium phosphate (pH7.4) and 2 M NaCl. The inner membranes were solubilized by incubation for 20 min at 277 K in 50 mM sodium phosphate (pH7.4) containing 2% TritonX-100. The outer membranes were washed with 50 mM sodium phosphate (pH7.4) and 5% glycerol, and then resuspended in 50 mM sodium phosphate (pH7.4), 300 mM NaCl, and 15% glycerol. Resuspended outer membranes were stored at 243 K prior to further purification.

OprN and OprJ were solubilized in 2% *n*-octyl-β-D-glucopyranoside (OG, Affymetrix). Insoluble material was removed by ultracentrifugation at 235,000g for 60 min. The supernatant was mixed with Ni-NTA agarose (Qiagen) equilibrated with the buffer containing 50 mM sodium phosphate (pH7.4), 300 mM NaCl, 20 mM imidazole, and 1.2% OG, and gently stirred at 277 K for 60 min. The resin was packed in an open column and washed with buffer containing 60 mM imidazole. OprN and OprJ were eluted with 250 mM imidazole. OprN was concentrated to 15mg/ml and dialyzed to 20 mM sodium phosphate (pH7.4) and 1.2% OG. OprJ was exchanged into buffer containing 20 mM sodium phosphate (pH7.4), 300 mM NaCl, and 1.2% OG using a PD-10 desalting column (GE Healthcare). Following elution, OprJ was concentrated to 8mg/ml. OprN and OprJ concentrations were estimated by measuring the absorbance at 280 nm. Purities of OprN and OprJ were assessed by SDS-PAGE (Figure 2.1).

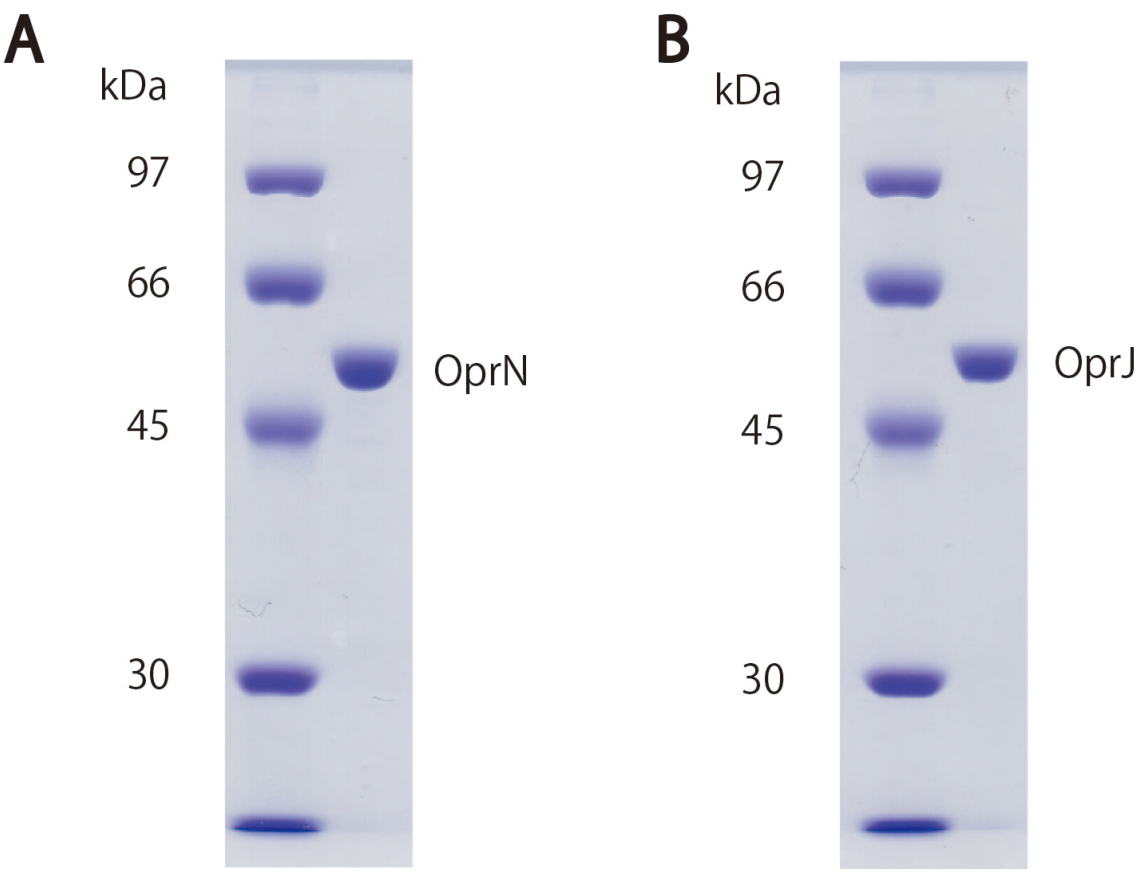

Figure 2.1 SDS-PAGE of OprN and OprJ

(A, B) SDS-PAGE of purified OprN (A) and OprJ (B).

2.3 Crystallization

Initial crystallization screenings were performed by the hanging and sitting drop vapor diffusion method using MPD Grid screen (Hampton Research) and MemGold2 (Molecular Dimensions). Initial crystals of OprN and OprJ were obtained in several conditions. The initial crystallization conditions were optimized by changing pH and precipitant concentration.

Best crystals of OprN were grown by the hanging drop vapor diffusion method at 293 K by mixing equal volumes of protein solution and reservoir, and obtained in two conditions. First and second conditions contain 100 mM sodium acetate (pH5.0) and 10% MPD (Figure 2.2A), and 100 mM sodium acetate (pH5.5), 6% PEG4000, and 800 mM sodium formate (Figure 2.2B), respectively. Crystals appeared in a few days and were grown within 1 week.

Best crystals of OprJ were obtained within drops mixing equal volumes of protein solution and reservoir containing 100 mM sodium acetate (pH6.0), 4% PEG4000, and 800 mM sodium formate (Figure 2.2C). The drops were equilibrated against the reservoir by the hanging drop vapor diffusion method at 293 K. Crystals appeared in a few days and were grown within 1 week.

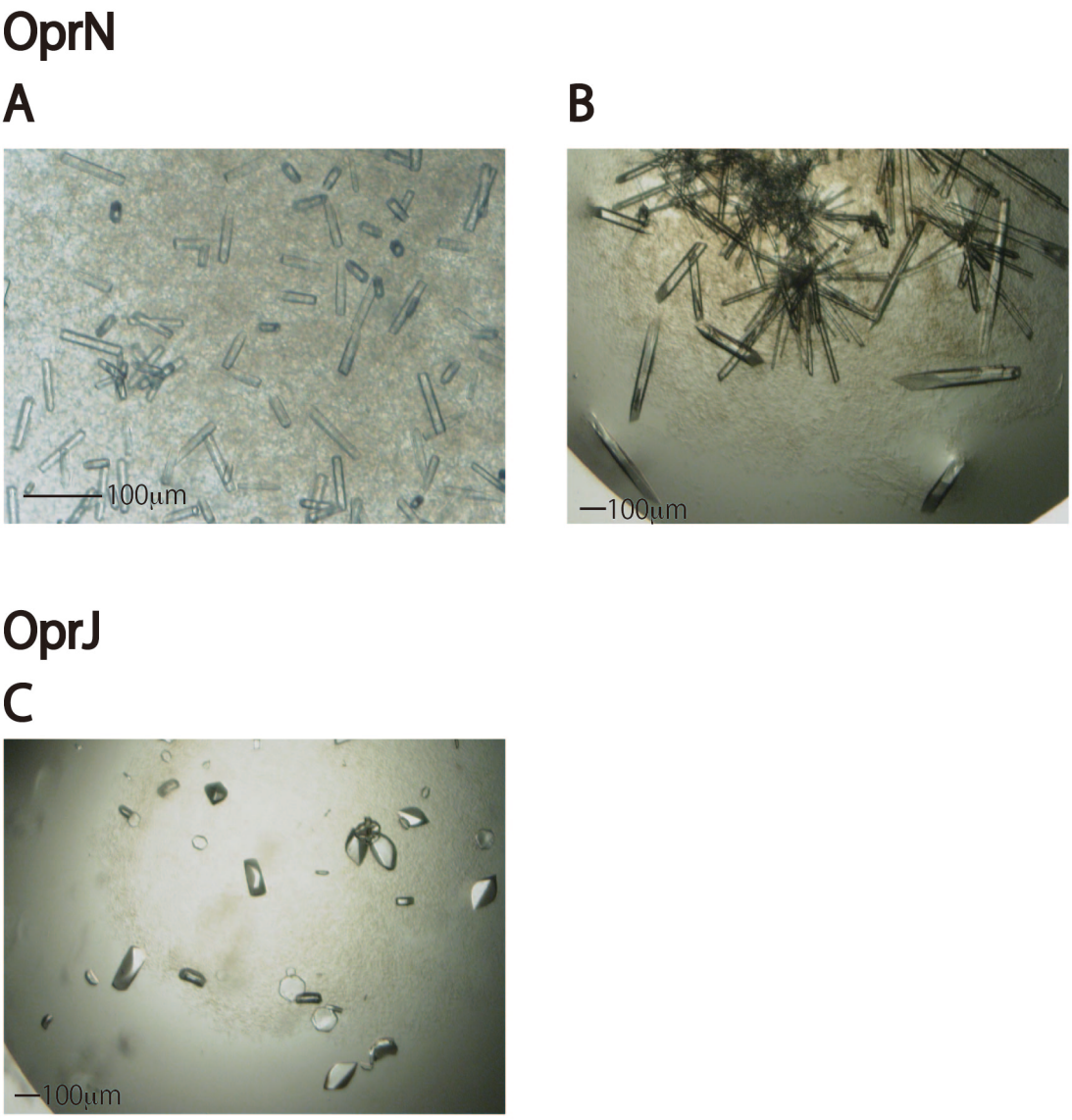

Figure 2.2 Crystals of OprN and OprJ

Each crystallization condition is 100 mM sodium acetate (pH5.0) and 10% MPD (A), 100 mM sodium acetate (pH5.5), 6% PEG4000, and 800 mM sodium formate (B), 100 mM sodium acetate (pH6.0), 4% PEG4000, and 800 mM sodium formate (C), respectively.

2.4 X-ray data collection

OprN crystals from crystallization condition using MPD were soaked in a cryoprotectant solution containing 100 mM sodium acetate (pH5.0), 25% MPD, and 1.2% OG, and lifted using LithoLoops (Protein Wave) for flash freezing in liquid nitrogen. OprN crystals from crystallization condition using PEG4000 were sequentially transferred to 1.2% OG and 30% glycerol in a reservoir solution using 5% stepwise increment of glycerol concentration, and lifted using LithoLoops (Protein Wave) for flash freezing in liquid nitrogen.

OprJ crystals were sequentially transferred to 1.2% OG and 30% glycerol in a reservoir solution using 5% stepwise increment of glycerol concentration, and lifted using LithoLoops (Protein Wave) for flash freezing in liquid nitrogen.

All diffraction data were collected on BL44XU at SPring-8 (Hyogo, Japan) with an MX300-HE CCD detector (Rayonix) at 100 K (Figure 2.3), and processed and scaled using the HKL2000 package (Otwinowski, Z. *et al.* 1997). Crystals of OprN from crystallization condition using MPD and PEG4000 belonged to *P*321 and *I*4 space groups, respectively. Cell parameters were $a=b=76.5$, $c=191.8$ Å for *P*321 and $a=b=257.5$, $c=81.8$ Å for *I*4. Crystals of OprJ belonged to $P2_12_12_1$ space group. Cell parameters were $a=86.3$, $b=92.4$, $c=252.8$ Å. Data collection statistics are summarized in Table 5.

A

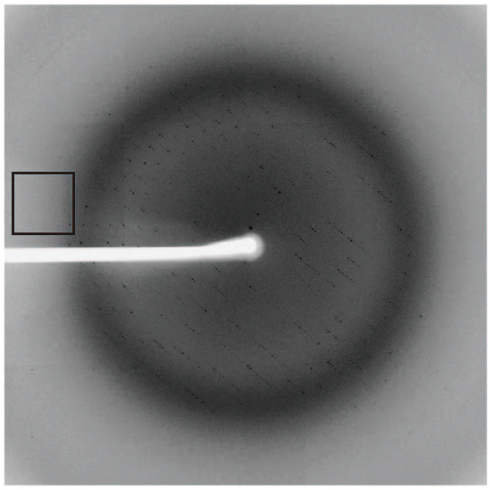

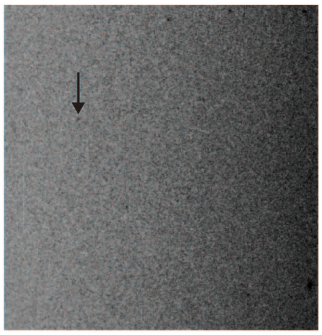

B

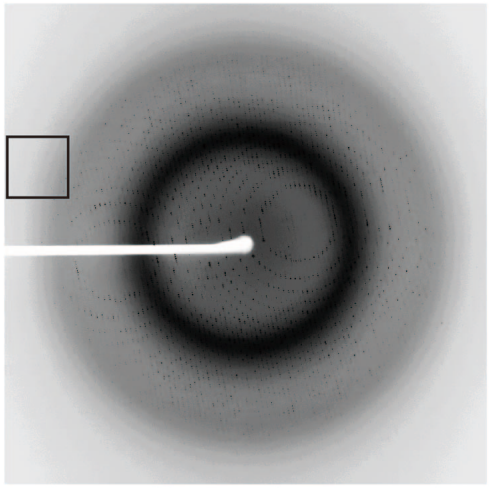

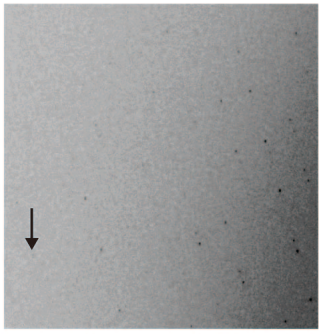

C

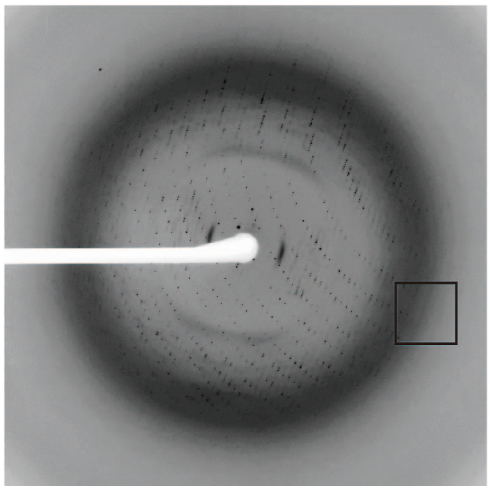

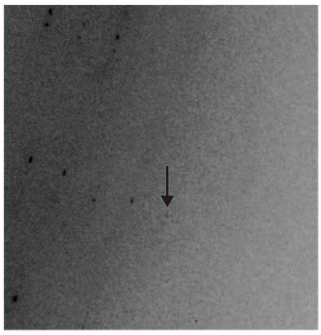

Figure 2.3 X-ray diffraction images of the crystals of OprN and OprJ

(A, B, C) Left and right sides show the overall diffraction pattern and zoom-up view of a box indicated at the left side, respectively. The arrow shows the diffraction spot of high resolution. (A), (B), and (C) is the diffraction images of trigonal crystal of OprN, tetragonal crystal of OprN, and orthorhombic crystal of OprJ, respectively.

Table 5 Data collection statistics of OprN and OprJ

	OprN(*I*4)	OprN(*P*321)	OprJ
Wavelength (Å)	0.90000	0.90000	0.90000
Space group	*I*4	*P*321	$P2_12_12_1$
Unit cell			
a, *b*, *c* (Å)	257.5, 257.5, 81.8	76.5, 76.5, 191.8	86.3, 92.4, 252.8
α, β, γ (°)	90, 90, 90	90, 90, 120	90, 90, 90
Resolution (Å)	50.00-1.69	50.00-2.70	50.00-3.10
	(1.72-1.69)[a]	(2.75-2.70)	(3.15-3.10)
R_{merge}[b]	0.068 (0.859)	0.164 (>1.0)	0.094 (0.780)
Unique reflections	297,648	18,601	36,834
$I/\sigma(I)$	22.9 (1.6)	17.1 (2.5)	20.9 (1.9)
Completeness (%)	99.5 (99.4)	100 (100)	97.2 (97.0)
Redundancy	3.6 (3.4)	10.9 (11.1)	4.5 (4.3)

[a]Values in the parentheses are for the highest resolution shells.

[b]$R_{merge} = \Sigma| I(hkl) - <I(hkl)>| / \Sigma I(hkl)$, where $I(hkl)$ is the observed intensity of individual reflection, and <I(hkl)> is the average intensity from multiple observations.

2.5 Structure determination

For OprN in the *P*321 space group [OprN(*P*321)], initial phase was determined by molecular replacement (MR) with MOLREP (Vagin, A. *et al.* 2010) in the CCP4 suite (Winn, M. D. *et al.* 2011) using the OprM crystal structure (PDB ID: 1WP1) (Akama, H. *et al.* 2004). The initial model was rebuilt using *Coot* (Emsley, P *et al.* 2010), before refinement in REFMAC5 (Murssudov, G. N. *et al.* 2011) and PHENIX (Adams, P. D. *et al*. 2010). The refinement statistics are summarized in Table 6. Ramachandran plot was calculated using *Rampage* (Lovell, S. C. *et al.* 2003) (Figure 2.4A).

For OprN in the *I*4 space group [OprN(*I*4)], initial phase was determined by MR with MOLREP (Vagin, A. *et al.* 2010) in the CCP4 suite (Winn, M. D. *et al.* 2011) using the crystal structure of OprN(*P*321). The initial model was rebuilt using *Coot* (Emsley, P *et al* 2010), before refinement in REFMAC5 (Murssudov, G. N. *et al.* 2011) and PHENIX (Adams, P. D. *et al.* 2010). The refinement statistics are summarized in Table 6. Ramachandran plot was calculated using *Rampage* (Lovell, S. C. *et al.* 2003) (Figure 2.4B).

For OprJ, initial phase was determined by MR with MOLREP (Vagin, A. *et al.* 2010) in the CCP4 suite (Winn, M. D. *et al.* 2011) using the OprM crystal structure (PDB ID: 1WP1) (Akama, H. *et al.* 2004). The initial model was rebuilt using *Coot* (Emsley, P *et al.* 2010), before refinement in REFMAC5 (Murshudov, G. N. *et al.* 2011) and PHENIX (Adams, P. D. *et al.* 2010). The refinement statistics are summarized in Table 6. Ramachandran plot was calculated using *Rampage* (Lovell, S. C. *et al.* 2003) (Figure 2.4C).

All structural figures were prepared using PyMol (DeLano W. L. 2002) and surface electrostatic potential was calculated by APBS (Baker, N. A. *et al.* 2001). Root mean square deviation (rmsd) values were calculated by SUPERPOSE (Krissinel, E. *et al*. 2004) in the CCP4 suite (Winn, M. D. *et al.* 2011).

Table 6 Refinement statistics of OprN and OprJ

	OprN(*I*4)	OprN(*P*321)	OprJ
Space group	*I*4	*P*321	$P2_12_12_1$
Resolution	50.00-1.69	50.00-2.70	50.00-3.10
R_{work}/R_{free}[a]	0.1601 / 0.1797	0.2315 / 0.2719	0.2686 / 0.3074
No. of atoms			
Protein	10,793	3,413	10,098
Ligand	379	0	0
Water	1885	0	0
Average B-values (Å^2)	26.5	49.4	113.2
Estimated standard uncertainty (e. s. u.)[b] (Å)	0.047	0.239	0.561
R.m.s. deviations			
Bond lengths (Å)	0.019	0.010	0.007
Bond angles (°)	1.973	1.336	1.124
Ramachandran plot (%)			
Most favored regions	99.0	98.2	98.2
Allowed regions	0.8	1.6	1.8
Outliners	0.2	0.2	0.1

[a]$R_{work} = \Sigma||F_{obs}| - F_{calc}| / \Sigma|F_{obs}|$, where $|F_{obs}|$ and $|F_{calc}|$ are the observed and calculated structure factor amplitudes, respectively. R_{free} was calculated with 5% of the data.

[b]Values were calculated based on maximum likelihood (Murshudov, G. N. *et al.* 2011).

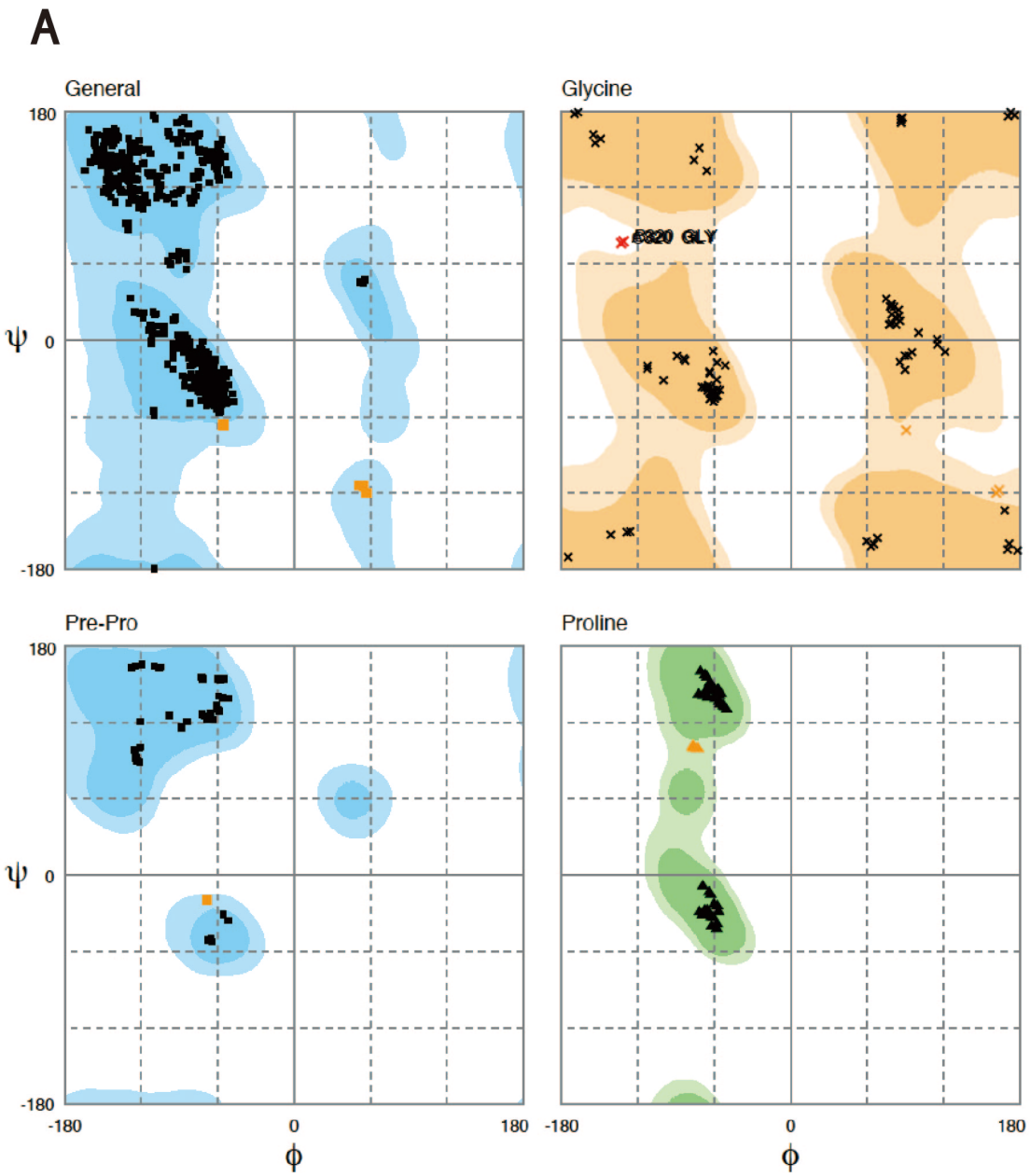

Figure 2.4 Ramachandran plots of OprN and OprJ structures

Figures show the phi and psi distribution for general case of non-Gly and non-Pro (left above), for Glycine (right above), for Pre-Proline (left bottom), and for Proline (right bottom). Preferred and allowed regions are shown in dark and light colors, respectively. General, Gly, Pre-Pro, and Pro are colored in blue, orange, blue, and green, respectively. (A) OprN(*I*4), (B) OprN(*P*321), (C) OprJ, respectively.

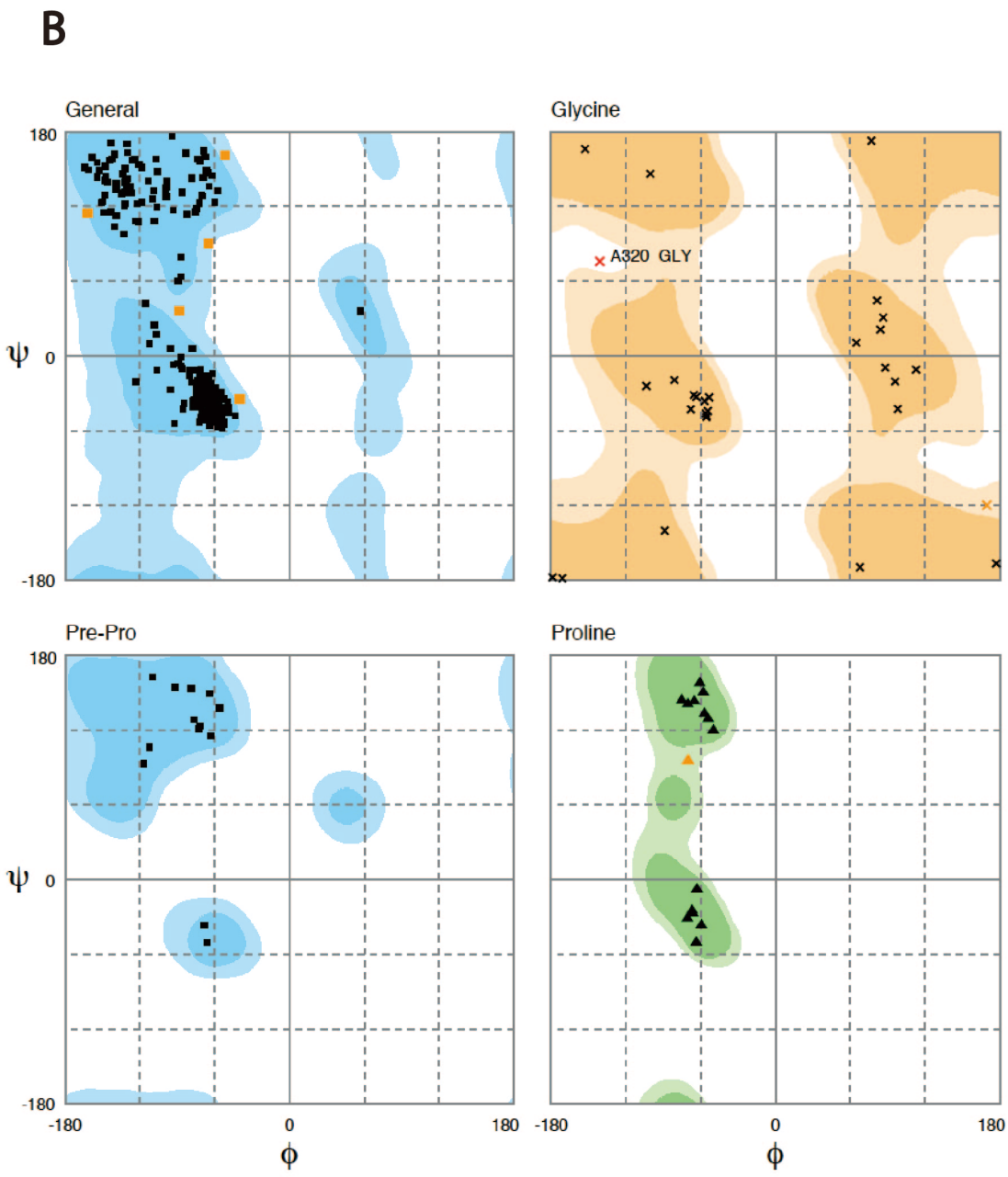

Figure 2.4 (continued)

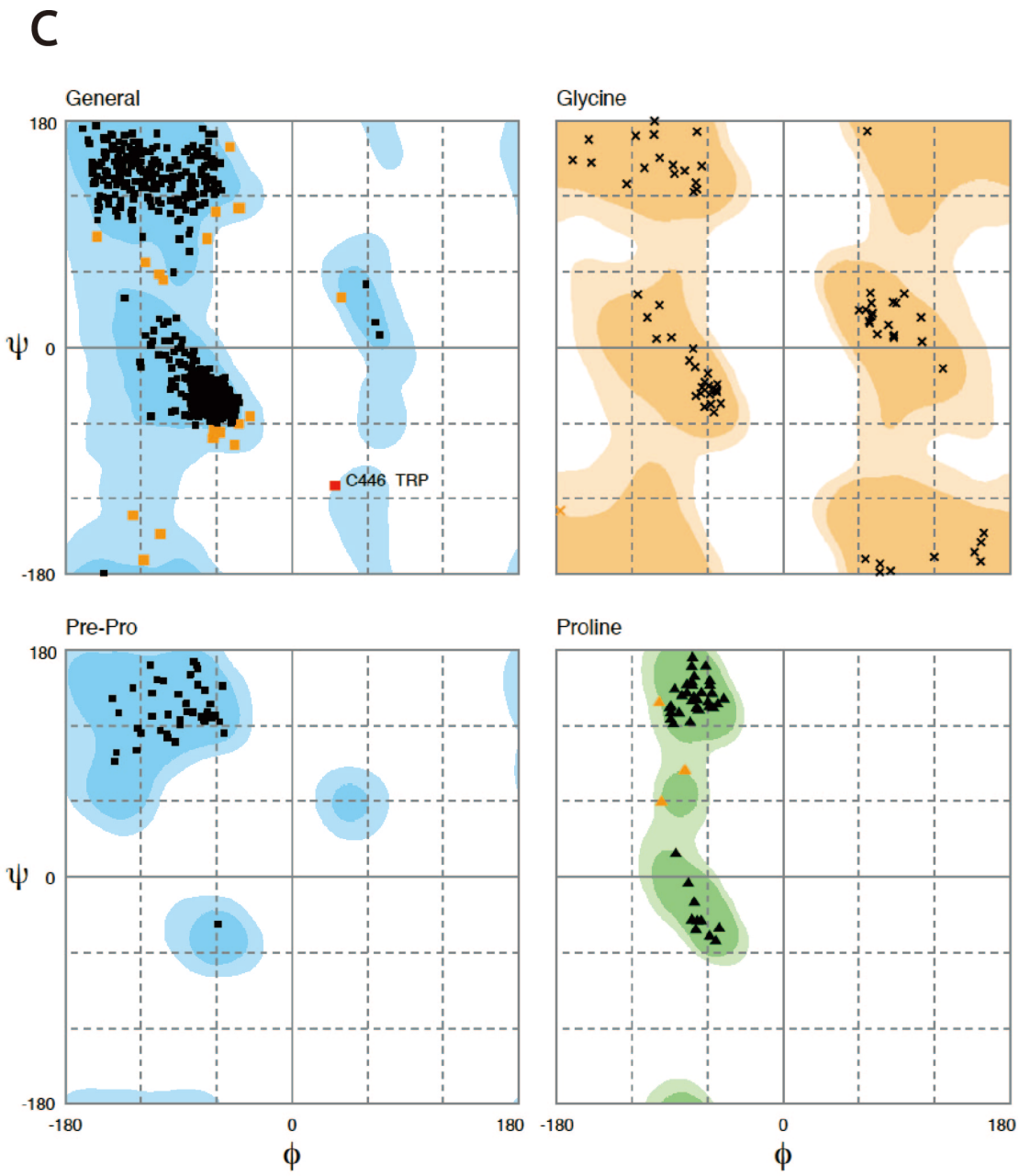

Figure 2.4 (continued)

Chapter 3
Result and Discussion

3.1 Overall crystal structures of OprN and OprJ

Crystal structure of OprN(*I*4) was determined at 1.69 Å resolution. The final model has been refined to R_{work} and R_{free} of 16.01% and 17.97%, respectively (Table 4 and Figure 3.1). One OprN trimer is contained in the asymmetric unit and protomer B includes 447 amino acid residues comprising 100% of total amino acid residues. In protomers A and C, a few C-terminal residues were disordered: 1–446 residues in the protomer A and 1–444 residues in the protomer C. Moreover, several C-terminal amino acid residues that translated from the vector's sequences can be built into the protomer B: Gly448, Se449, and His450. These ordered amino acid residues interacted with Arg181, Glu185, Arg188, and Glu195 of a crystallographic symmetry mate. The OprN trimer forms an α-barrel and a β-barrel with a total length of about 130 Å (Figure 3.1).

Crystal structure of OprJ was determined at 3.10 Å resolution. The final model has been refined to R_{work} and R_{free} of 26.86% and 30.74%, respectively (Table 4 and Figure 3.3). One OprJ trimer is contained within the asymmetric unit, and each protomer include 430–446 amino acid residues comprising 93.5–97.0% of total amino acid residues, with the exception of Gly20–Thr32 in protomer A, Ala22–Ala29 in protomer B, and Ala21–Ala29 in protomer within the equatorial domain and several C-terminal amino acid residues of all protomers, which are disordered. The OprJ trimer forms an α-barrel and a β-barrel with a total length of about 135 Å (Figure 3.2).

The overall structures of OprN and OprJ have conserved folds in the OMF structures (Figure 3.3). The β-barrel and α-barrel domains consist of four anti-parallel β-strands (S1, S2, S3, and S4) and six helices, respectively. In particular, two of long helices (H3 and H7) in the α-barrel domain extend across the entire length of the periplasmic region,

and short helices stack end-to-end to form pseudocontinuous helixes (H2 and H4 or H6 and H8). The α-barrel domain is formed by outer coiled-coil helices (H3/H4) and inner coiled-coil helices (H7/H8), and stabilized by these coiled-coil interactions between each other. The equatorial domain is located in the middle of the α-barrel domain, and consists of two short helices (H1 and H5) and a large loop between H4 and H5.

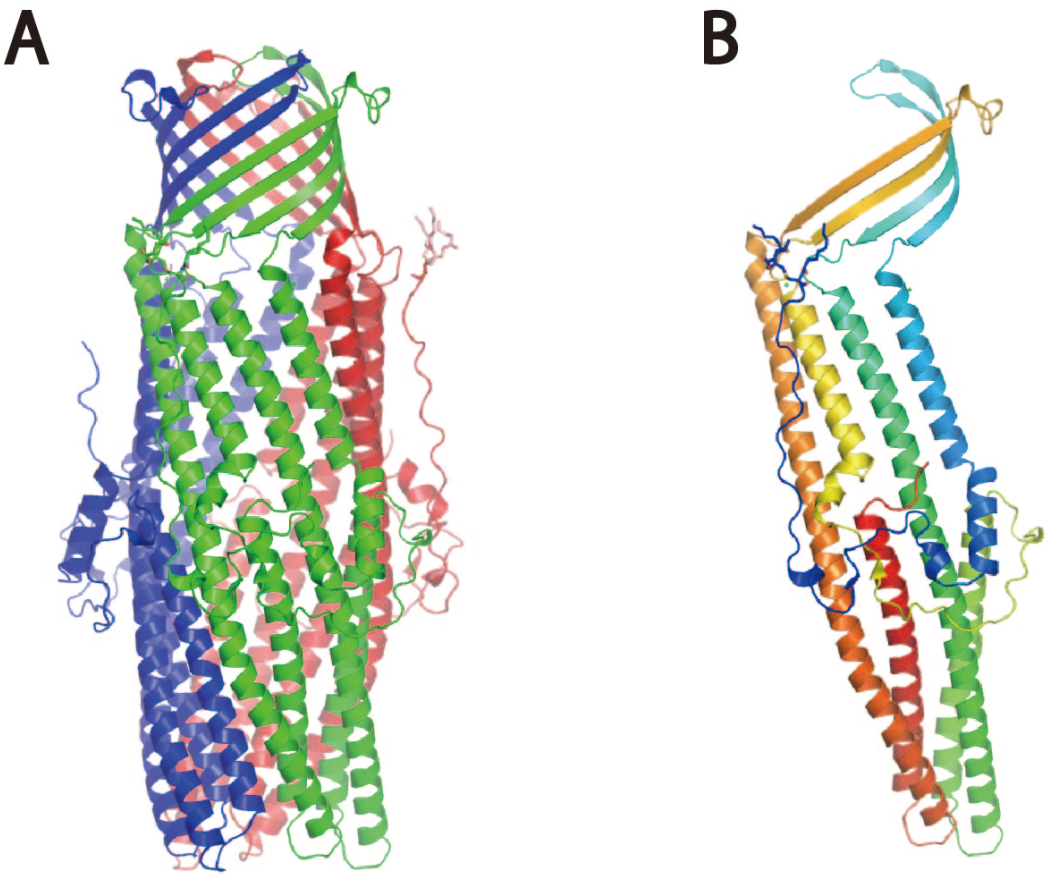

Figure 3.1 Crystal structure of OprN

(A, B) Ribbon diagrams of the OprN trimer (A) and monomer (B) viewed from the transmembrane plane. The monomer is colored using a rainbow gradient from N- (blue) to the C-terminus (red).

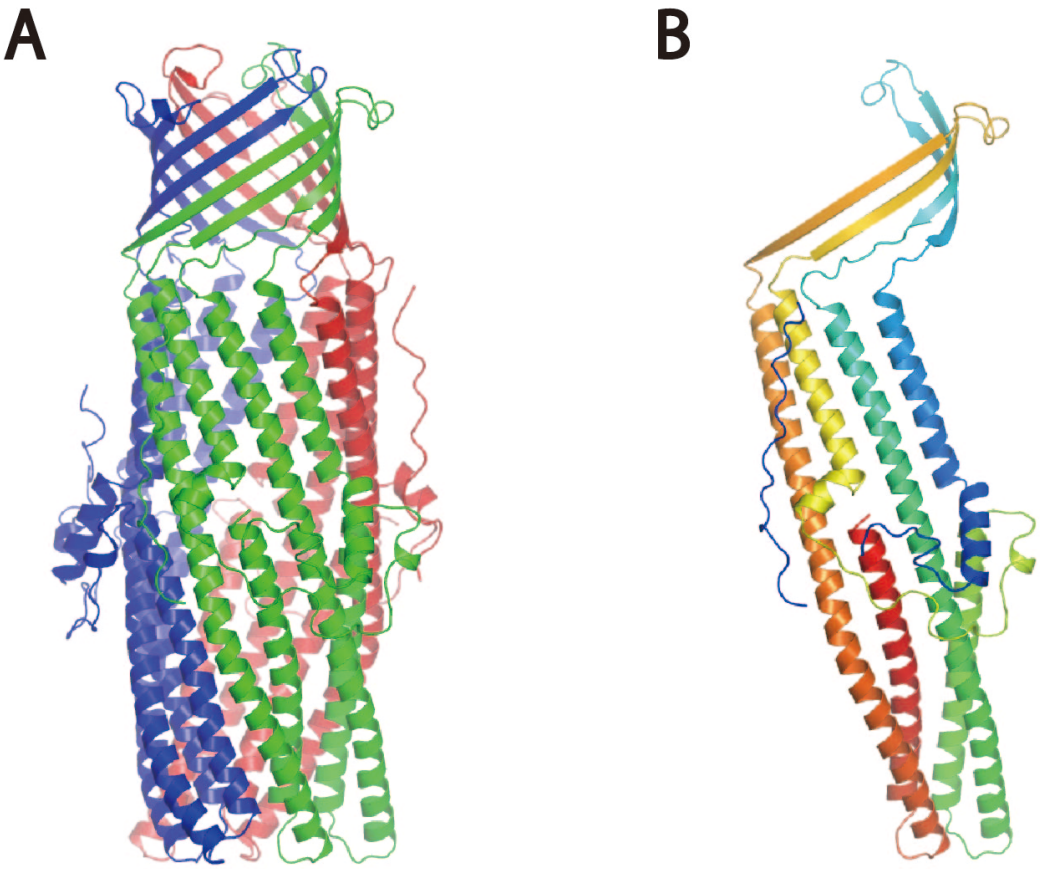

Figure 3.2 Crystal structure of OprJ

(A, B) Ribbon diagrams of the OprJ trimer (A) and monomer (B) viewed from the transmembrane plane. The monomer is colored using a rainbow gradient from N- (blue) to the C-terminus (red).

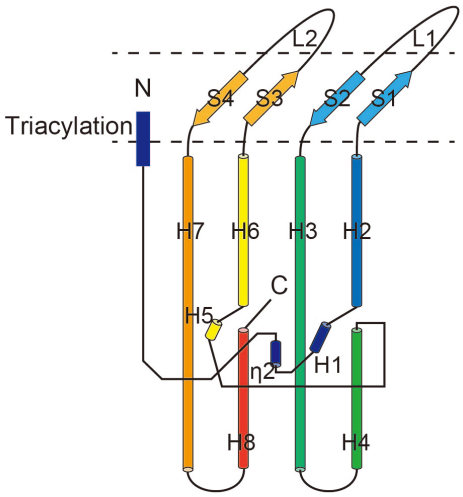

	OprN	OprJ	OprM
η2	W34-F38	W35-F38	W40-F43
H1	P41-G53	A42-N54	P47-N59
H2	R55-R78	R56-A77	R61-A82
H3	R123-D189	R126-A193	R131-D197
H4	E195-L229	A198-L233	A203-L238
H5	P258-R264	P261-R267	D267-R271
H6	P266-A287	P269-A290	P273-A294
H7	A327-E399	R335-E401	S339-R405
H8	F404-L439	H407-L442	Y411-L446
S1	V81-Q95	N84-Q94	I88-L99
S2	T99-E117	E105-L121	A110-L126
S3	R292-A303	R295-S306	S299-S310
S4	R315-W325	R318-F331	G322-F335

Figure 3.3 Topology of OprN, OprJ, and OprM

(*Left*) The topology is based on the OprN, OprJ, and OprM crystal structures. Secondary structural elements are shown: H, helices; S, strands; L, loop. (*Right*) The table shows ranges of residues for each secondary structural element.

3.2 Symmetric and asymmetric trimer of OprN

Crystal structure of OprN(*P*321) space group was also determined at 2.70 Å resolution. The final model has been refined to R_{work} and R_{free} of 23.15% and 27.19%, respectively (Table 4). One OprN protomer is contained within the asymmetric unit, and includes 444 amino acid residues comprising 99.3% of total amino acid residues. The monomers of OprN trimer are related by a crystallographic 3-fold axis. Hence, the protomer in OprN(*P*321) exhibits 3-fold symmetry, whereas the protomers in OprN(*I*4) form an asymmetric trimer. Structural alignments of each protomer resulted in rmsd values ranging from 0.31 to 0.54 Å between each protomer in OprN(*I*4), and from 0.48 to 0.54 Å between each protomer in OprN(*I*4) and OprN(*P*321) (Figure 3.4A). These results indicate that the crystallization conditions may not significantly affect the overall structure of OMFs. This is supported by the fact that the rmsd values between the protomers within symmetric and asymmetric trimer of OprM is range from 0.37 to 0.45 Å (Akama, H. *et al.* 2004; Phan, G. *et al.* 2010).

In OprN and OprJ, however, there are local structural differences at the extracellular loop of the β-barrel domain, the periplasmic tip of the α-barrel domain, and the large loop between H4 and H5 (Figure 3.4). These local structural differences mainly result from high temperature factors (Figure 3.5). At the periplasmic tip of the α-barrel domain of OprN(*I*4), crystal contacts also caused structural differences (Figure 3.6). In protomer A, Glu399 in a loop between H7 and H8 is forced out to avoid clashing with Ser52, which is related by a crystallographic symmetry (Figure 3.6). As a result, the loop formed by Glu399–Asp403 is shifted, but all H7 and H8 are in the same position.

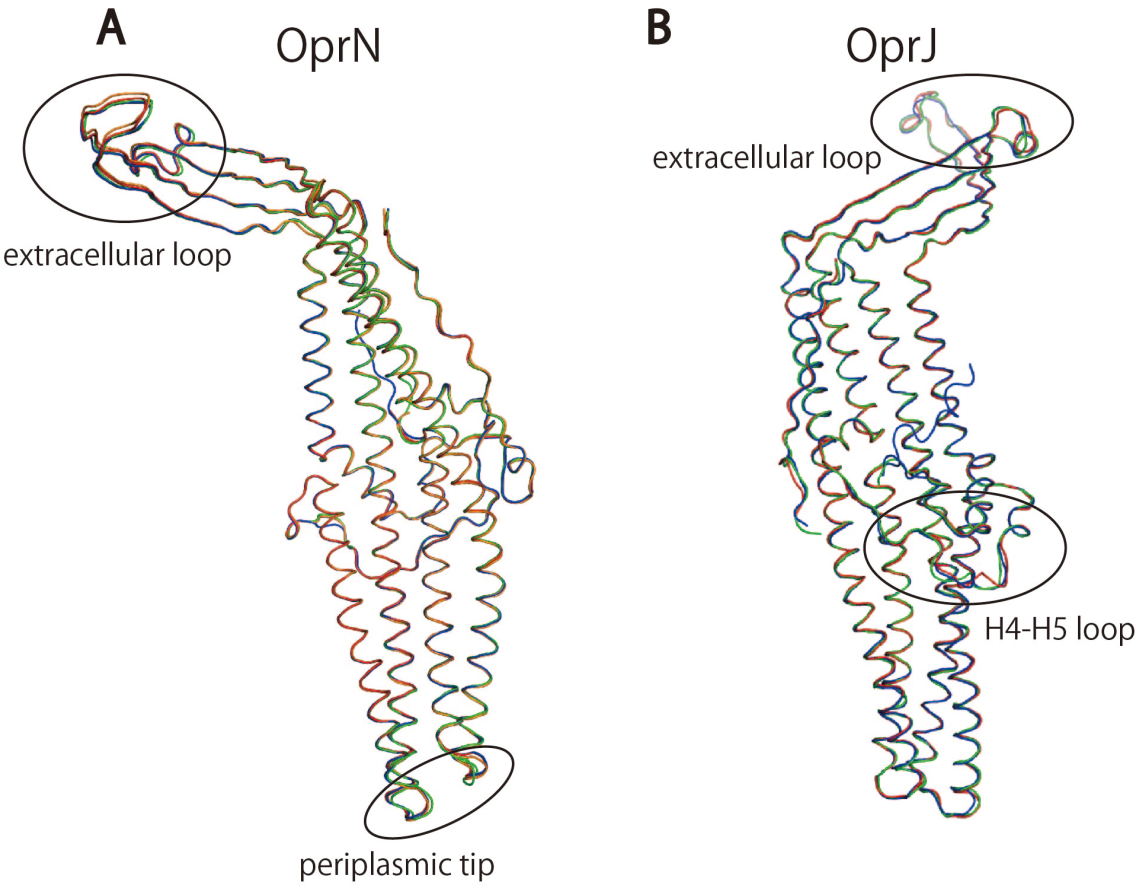

Figure 3.4 Superposition of each protomer of OprN or OprJ

(A) Superposition of each protomer of OprN(*I*4) and OprN(*P*321). The protomers of OprN(*I*4) and OprN(*P*321) are colored in green, blue, red, and orange, respectively. (B) Superposition of each protomer of OprJ. Each protomer is colored in green, blue, and red, respectively.

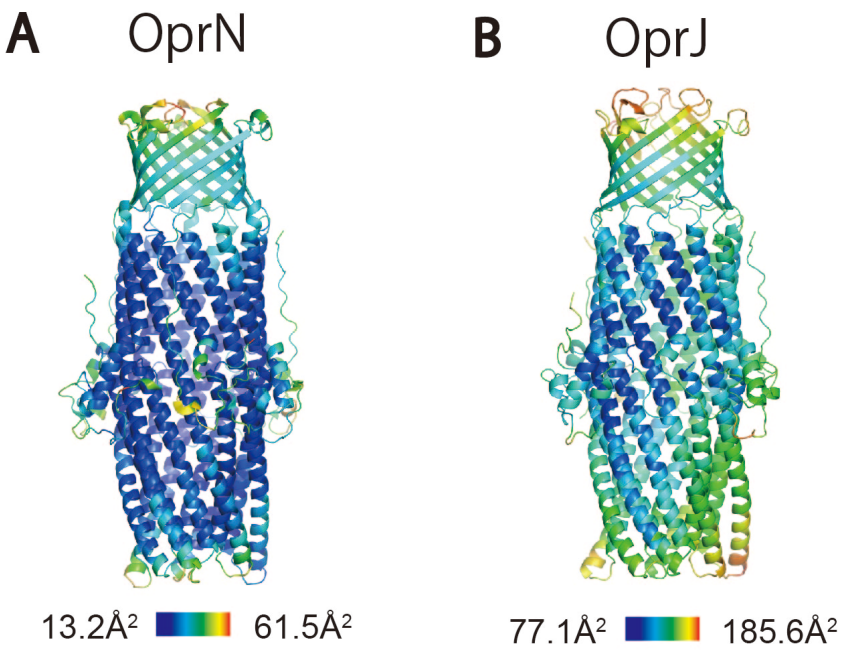

Figure 3.5 Temperature factors of OprN or OprJ

(A, B) The temperature factors of OprN(*I*4) (A) and OprJ (B) are represented in rainbow colors.

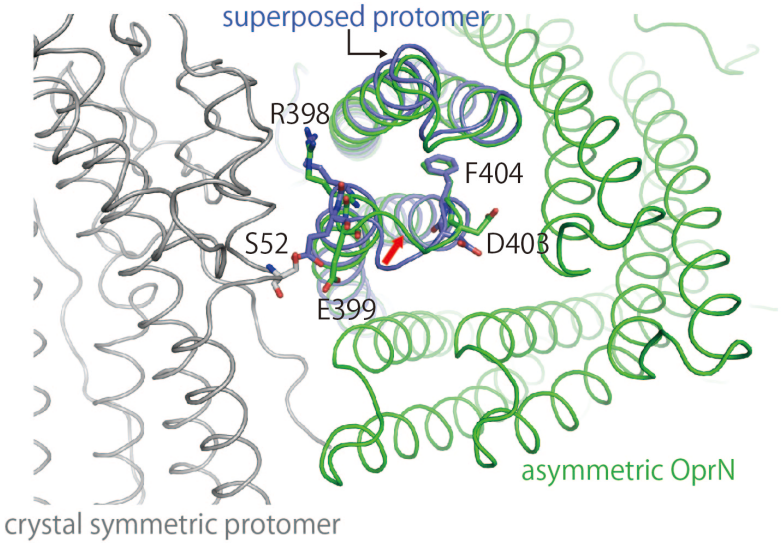

Figure 3.6 Crystal contact of asymmetric OprN

3.3 Modification of N-terminal cysteine

OprN and OprJ are functional homolog of OprM. OprM is a lipoprotein and the N-terminal cysteine may be important for anchoring to the outer membrane (Nakajima, A. *et al.* 2000). The crystal structure of OprM showed weak electron density for a fatty acid at N-amine and S-thiol in Cys1, and the N-terminal end extends toward the β-barrel domain (Akama, H. *et al.* 2004). These results suggest that OprM is most likely modified by a fatty acid at its N-terminal cysteine. The N-terminal cysteine is conserved in both OprN and OprJ, and the crystal structures of OprN and OprJ revealed that the both N-terminal ends extend toward the β-barrel domain. In the crystal structure of OprN(*I*4), clear electron density for a fatty acid was observed at the N-terminal cysteine. The electron density map revealed N-acyl and S-diacylglycerol functional groups covalently linked to Cys1 (Figure 3.7A). Although the crystal structure of OprN(*I*4) was determined at 1.69 Å resolution, the acyl chains on protomer B could not be assigned. Moreover, the acyl chains on protomer A and C were partial, and the alky groups following the 5–8th carbon atoms of all acyl chains were disordered. The most likely reason for the disordered alkyl groups is flexibility. Higher resolution structure is needed to determine the position of the full acyl chains. In deed, modifications of OprN(*P*321) and OprJ at their N-terminal cysteine could not be determined due to the low-resolution structure, but their cysteine may be modified in a similar way to that of OprN(*I*4) considering the similarities in amino acid sequence and crystal structures of their N-terminal ends extending toward the β-barrel domain.

Crystal structures of OMFs with different N-terminal modifications have been reported (Kulathila, R. *et al.* 2011; Lei, H. T. *et al.* 2014; Su, C. C. *et al.* 2014; Monlezun, L. *et al.* 2015), and the N-terminal modification type has not yet been determined based on the crystal structure. In this study, *E. coli* was used as the expression system of OprN and OprJ, but their native host is *P. aeruginosa*. This raises a

question of how the triacylation of the crystal structure of OprN(*I*4) is consistent with its native modification. In *E. coli*, outer membrane lipoproteins are synthesized in its cytosol as precursors with a signal peptide. Then, they are translocated to the periplasmic side of the inner membrane, and processing into mature forms is performed with three enzymes, which are phosphatidylglycerol-prolipoprotein diacylglycerol transferase (*lgt*), lipoprotein signal peptidase, and apoliporotein N-acyltransferase (*lnt*) (Sankaran, K. *et al.* 1994; Okuda, S. *et al*. 2011). Among these enzymes, Lgt stimulates a reaction forming a thioether linkage between the N-terminal cysteine and diacylglycerol, and Lnt an acylation at the N-terminal cysteine. Then, the mature lipoproteins are translocated and inserted to the outer membrane by Lol system, involving LolA, LolB, LolC, LolD, and LolE (Okuda, S. *et al.* 2011). In *P. aeruginosa*, the enzymes and Lol system are conserved (Remans, K. *et al.* 2010). In particular, Lgt and Lnt have high amino acid sequence identity of 55.6% and 40.5%, respectively. These results indicate that lipoproteins of *P. aeruginosa* may be modified in a similar way to those of *E. coli*, that the triacylation of the crystal structure of OprN(*I*4) may be consistent with the native modification. By comparing with crystal structure modified at the N-terminal cysteine, the modification of the crystal structure of OprN(*I*4) is similar to that of CusC (Kulathila, R. *et al.* 2011) (Figure 3.7B and 3.7C). This result suggests that the N-terminal cysteine of OMF may be triacylated and that acyl chains may be inserted into the outer membrane.

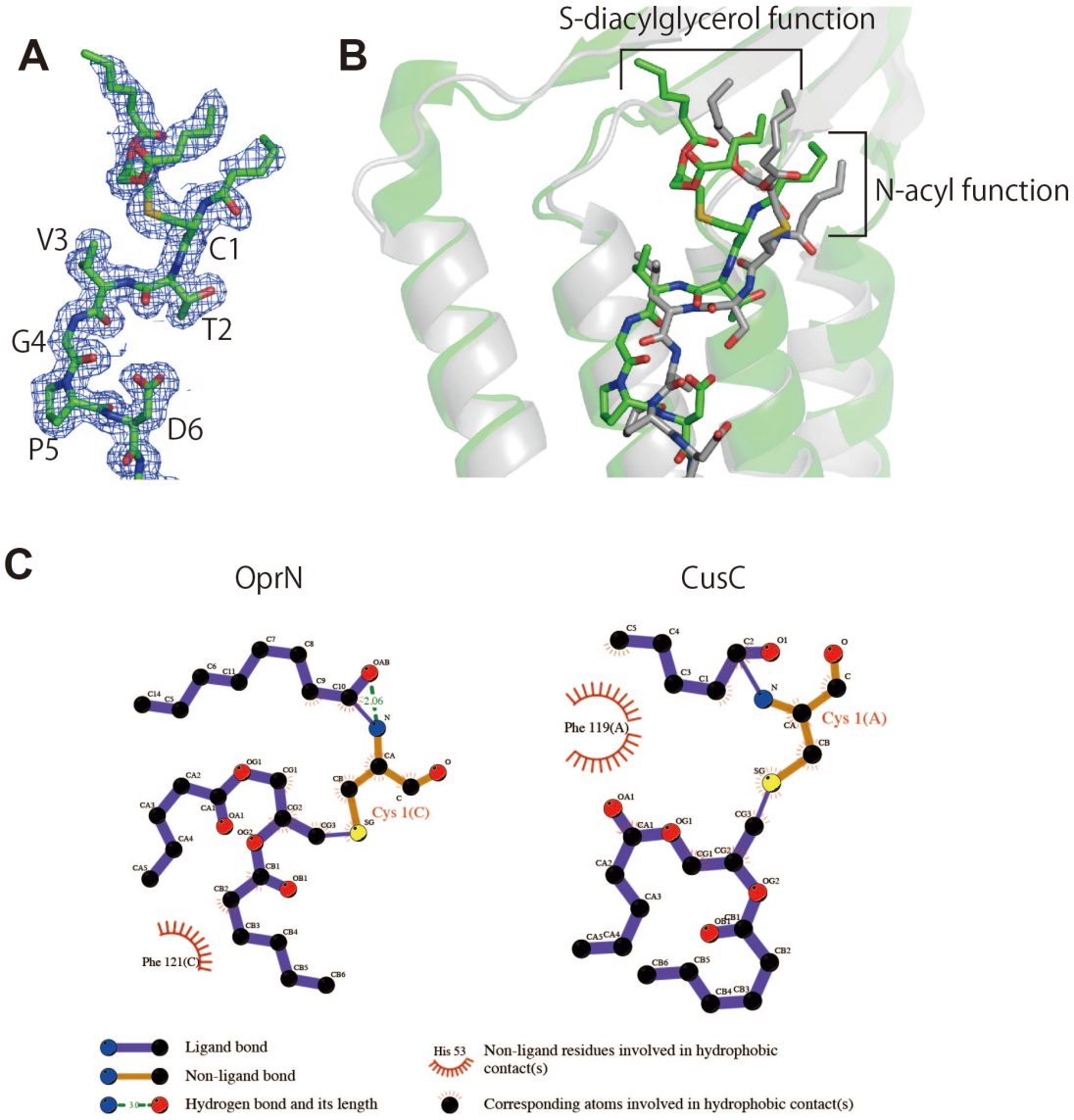

Figure 3.7 Triacylation at the N-terminal cysteine of OprN

(A) $2m|F_o|$-$D|F_c|$ electron density of acyl chains, Cys1, Thr2, Val3, Gly4, Pro5, and Asp6 are contoured at 1.0 σ. Carbon, nitrogen, oxygen, and sulfur atoms are colored in green, blue, red, and yellow, respectively. The N-terminal cysteine is triacylated by N-acyl and S-diacylglycerol functions. (B) Cartoon model showing superposition of OprN and CusC (PDB ID: 3PIK). CusC and its carbon atoms are shown in gray. Other atoms are colored as in (A) (C) Schematic representations of triacylation of OprN (*Left*) and CusC (*Right*) were calculated by LIGPLOT (Wallace, A. C. *et al.* 1996)

3.4 Ligands in the crystal structure of OprN(*I*4)

Since the crystal structure of OprN(*I*4) was determined at 1.69 Å resolution, several ligands and a large number of water molecules were clearly observed (Figure 3.8). The crystal structure of OprN(*I*4) contained ten acetate ions, three sodium ions, twenty-one formic acid molecules, fourteen glycerol molecules, and eight OG molecules.

Comparing the binding of each OG in the crystal structure of OprN(*I*4), a few of OG were bound to a same position within each protomer. In this site, side chain nitrogen ($N^{\eta 1}$ and $N^{\eta 2}$) atoms of Arg334 interacted with water molecules and oxygen atoms within OG molecules (Figure 3.9). Furthermore, acyl chains of OG molecules extended toward hydrophobic regions formed by Phe290, Pro291, Trp325, and Phe328. Among these residues, Phe290, Pro291, and Phe328 are conserved in OprN, OprJ, and OprM. In contrast, the hydrophobicity of Trp325 in OprN is similar to the residues in OprJ and OprM (L328 in OprJ and L332 in OprM). Basic and hydrophobic residues may be important for interactions with phospholipids in the outer membrane.

The ELDLFGR motif of OprN was near the N-terminal cysteine and fatty acids (Figure 3.10). Thus, this motif may be important for localization to the outer membrane. Since side chains of Glu117 and Arg123 faced to the inside of OprN, these residues may not interact with phospholipids. In OprM, mutations for these corresponding residues, which are Glu125 and Arg131, had no effect on the function of MexAB-OprM (Li, X. Z. *et al.* 2001). In contrast, side chains of Asp119 faced to the outside of OprN, and interacted with water molecules and Arg125. Arg125 is a residue following the ELDLFGR motif and fixed a position of the N-terminal end by interacting with the oxygen atom of Cys1 and side chain oxygen (O^{γ}) atom of Thr2. In OprJ and OprM, Arg125 corresponds to Lys128 and Arg133, respectively. These basic residues may be also important for interactions with phospholipids in the outer membrane.

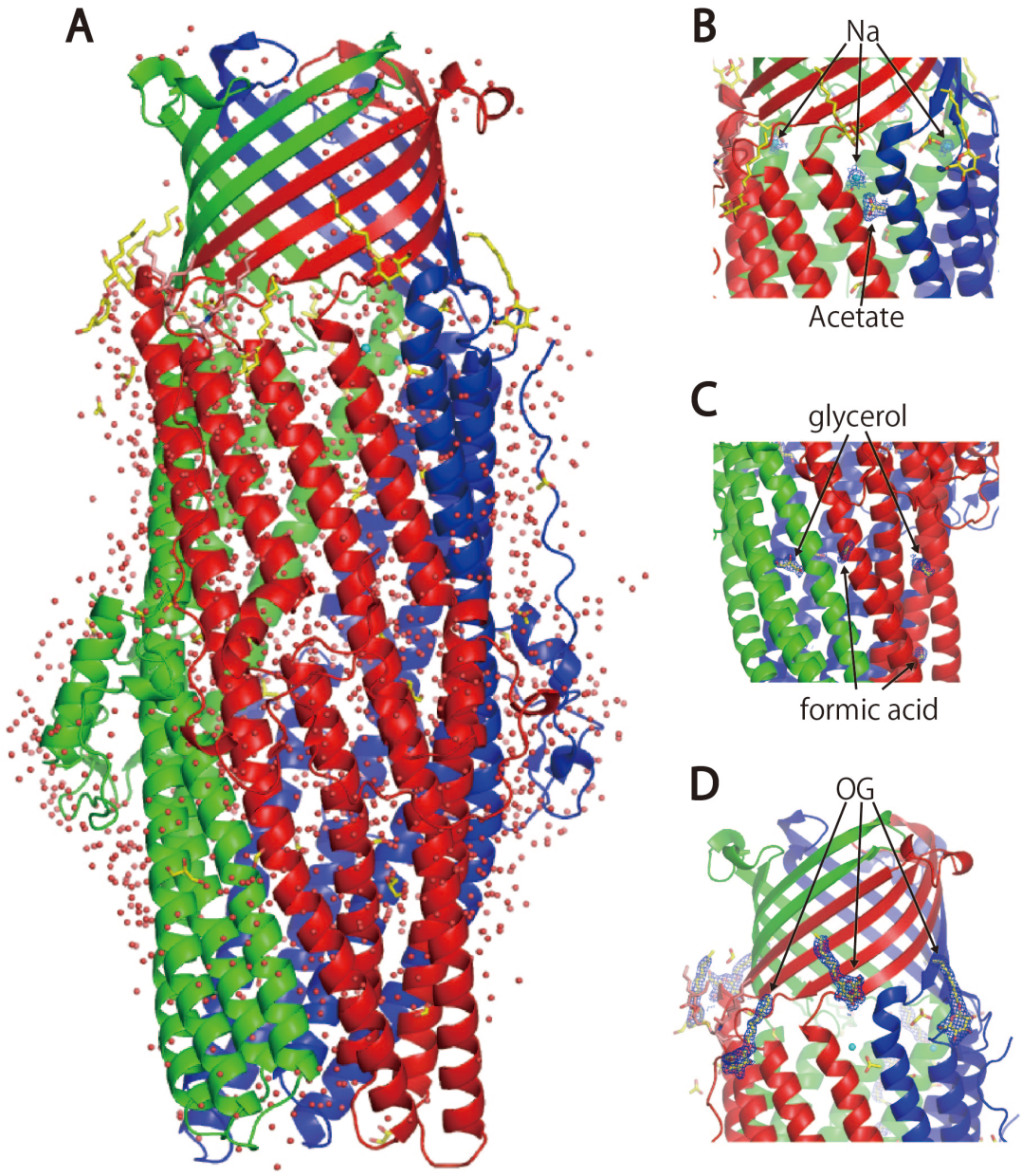

Figure 3.8 Ligands in the crystal structure of OprN(*I*4)

(A) Ligands, sodium ions and water molecules are shown in stick model, cyan and red sphere, respectively. Carbon and oxygen atoms are colored in yellow and red, respectively. (B, C, D) Close-up view of the binding site of sodium and acetate ion (B), glycerol and formic acid (C) and OG (D). $2m|F_o|$-$D|F_c|$ electron density of each ligand is contoured at 1.5 σ.

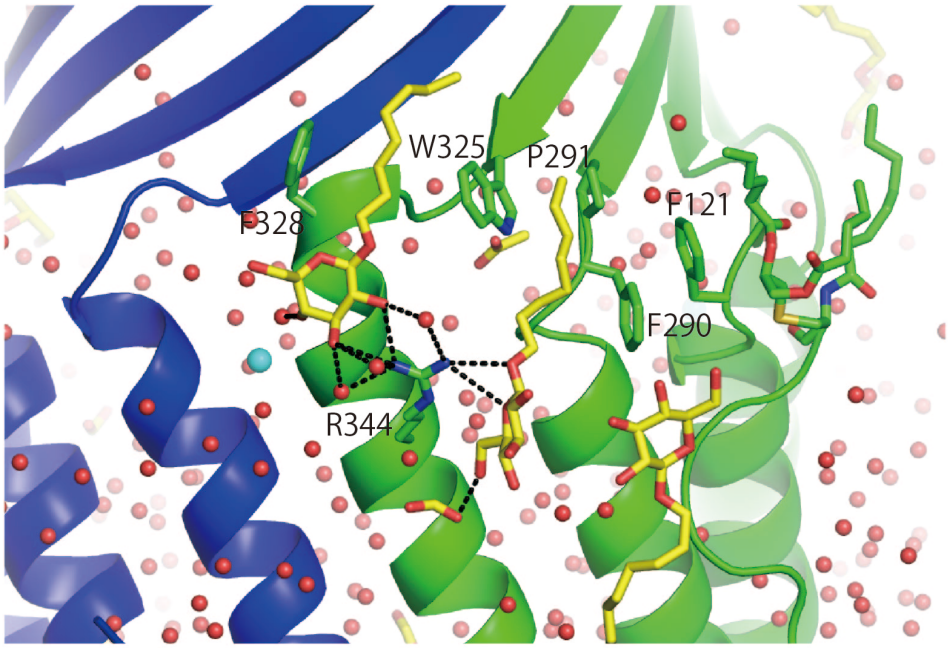

Figure 3.9 Close-up view at Arg334 of OprN

Atoms of OprN and ligands are colored as in Figure 3.7 and Figure 3.8, respectively. Hydrogen bonds are shown as black dash lines.

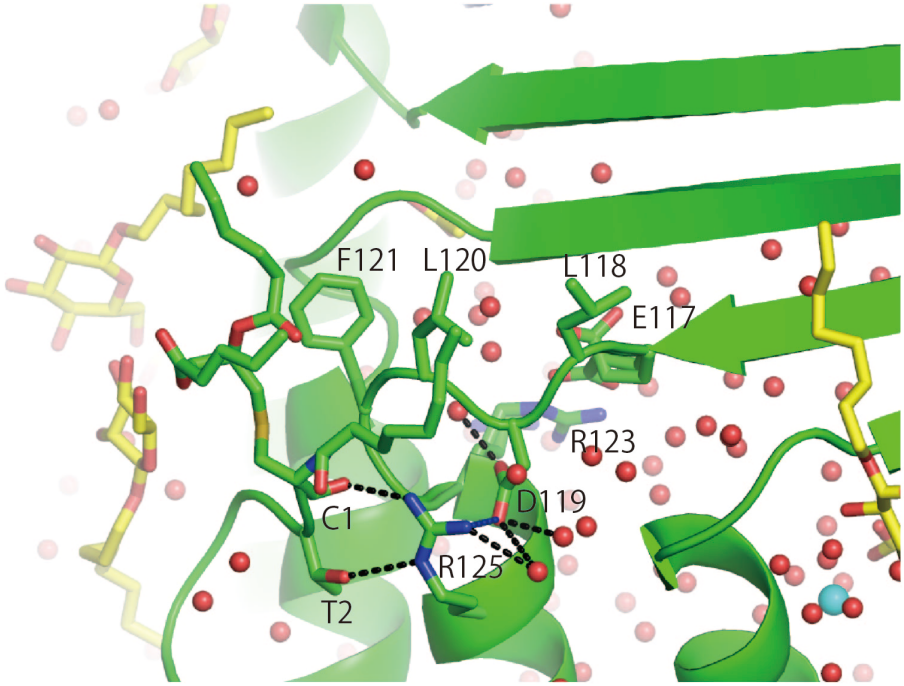

Figure 3.10 Close-up view at the ELDLFGR motif

Atoms of OprN and ligands are colored as in Figure 3.7 and Figure 3.8, respectively. Hydrogen bonds and salt bridge are shown as black and blue dashed lines, respectively.

3.5 Structural comparison of OprN, OprJ, and OprM

Superposing the OprN, OprJ, and OprM (Akama, H. *et al.* 2004) crystal structure revealed that OprJ is structurally more similar to OprM than to OprN. The overall rmsd values for Cα atoms are 1.02 Å, 1.41 Å, and 1.50 Å between OprJ and OprM, OprN and OprM, and OprN and OprJ, respectively. This result is consistent with the high similarity in amino acid sequence between OprJ and OprM (59.1%). Moreover, the superposition also revealed structural differences at the equatorial domain and the periplasmic end of α-barrel domain (Figure 3.11).

The overall structures of equatorial domains were dissimilar among OprN, OprJ, and OprM (Figure 3.11). The overall rmsd values for Cα atoms of equatorial domains were 1.33 Å, 2.81 Å, 2.97 Å between OprJ and OprM, OprN and OprM, OprN and OprJ, respectively. The large rmsd values were mainly attributed to the structural differences of loop between H4 and H5 (Figure 3.11 and 3.12). In addition, this loop shows low amino acid sequence similarities between OprN, OprJ, and OprM (Figure 1.5). Yamanaka *et al.* showed that the exchanging the H4–H5 loop of TolC to that of other OMF decreases susceptibility for novobiocin, that the structure and amino acid sequence of this loop affect the transport activity of AcrAB-TolC (Yamanaka, H. *et al.* 2007) Therefore, the H4–H5 loop may have a unique structure dependent on each OMF, and the structural difference of its loop may be important for the *in vivo* function of each tripartite efflux pump.

Although the overall structures of equatorial domains had large structural differences, η2, H1, and H5, which are components of the equatorial domain, located at similar positions (Figure 3.12). Furthermore, η2 and H1 contains important residues. Yamanaka *et al.* showed that Leu3 and Leu412 in TolC, which form hydrophobic interactions with each other, are important for the protein's ability to transport novobiocin *in vivo* (Yamanaka, H. *et al.* 2002; Yamanaka, H. *et al.* 2004). Leu3, which is located on H1, is

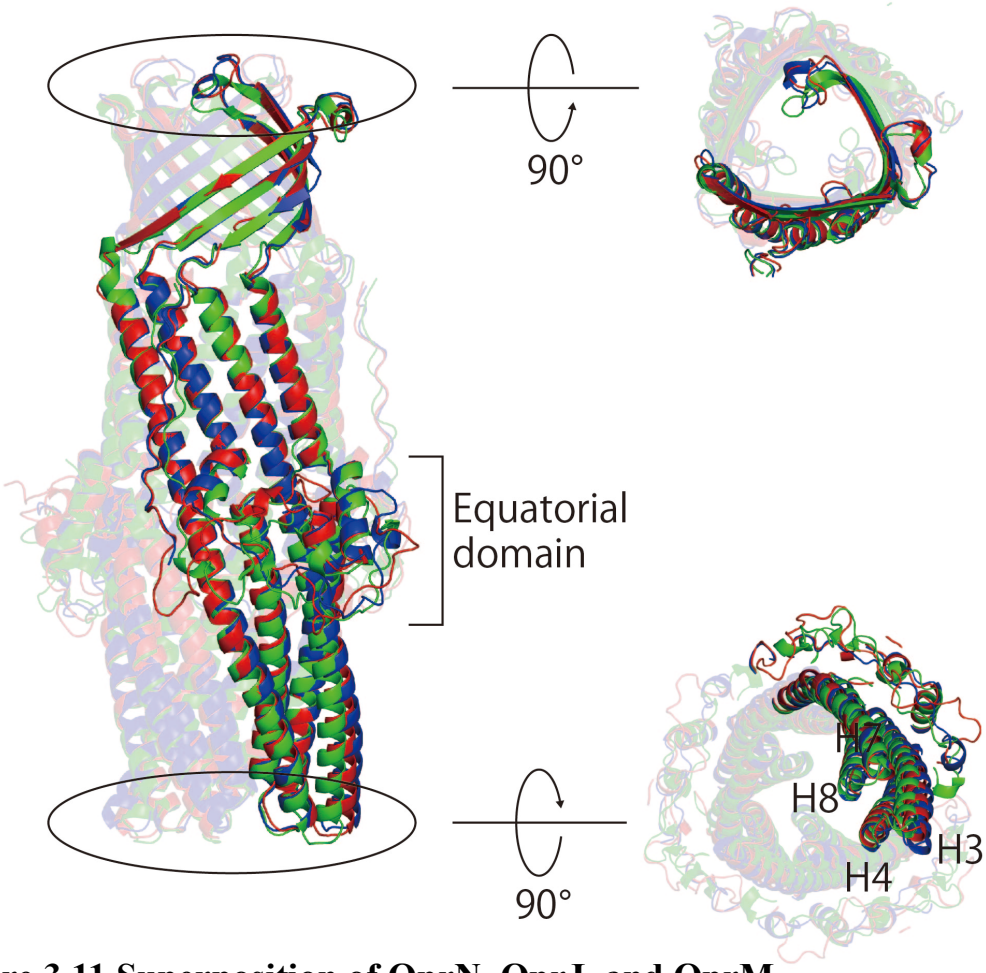

Figure 3.11 Superposition of OprN, OprJ, and OprM

Side (*left*), extracellular (*right above*), and periplasmic (right bottom) views are represented. OprN, OprJ, and OprM are colored in green, blue, and red, respectively.

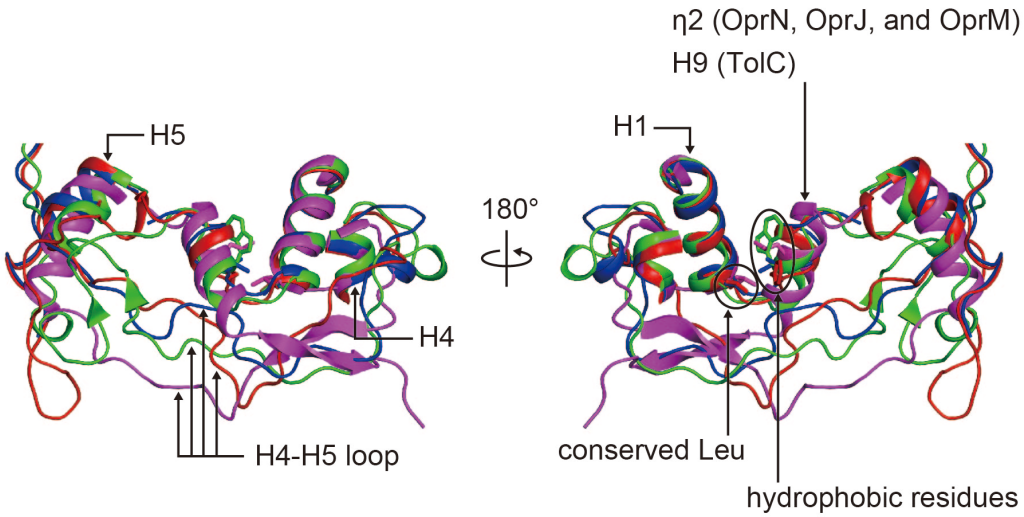

Figure 3.12 Superposition of the equatorial domain

OprN, OprJ, and OprM are colored as in Figure 3.11. TolC (PDB ID: 1EK9) is colored in magenta.

conserved in OprN as Leu43, in OprJ as Leu44, and in OprM as Leu49 (Figure 3.12). Leu412 is located on H9 of TolC, which corresponds to η2 in OprN, OprJ, and OprM, and only the hydrophobicity of the residue is similar (Trp35 in OprN, Ile39 in OprJ and Phe44 in OprM) (Figure 3.12). The hydrophobic interaction between Leu on H1 and hydrophobic residue on η2 may be important for maintaining the structure of the equatorial domain, and the stable structure of the equatorial domain may be important for *in vivo* function of the tripartite efflux pump.

In contrast to the large structural differences observed in the loop between H4 and H5, those at the periplasmic end of α-barrel domain are small and local. The positions and tips of H3 helices are inconsistent with one another, while those of H4, H7, and H8 helices are consistent (Figure 3.11 and 3.13A). In particular, H3 helices of OprN and OprM were tilted toward their intraprotomer grooves at the middle position of H3 helices (Figure 3.13A). The tilt angles of H3 helices are about 2.3° in OprM and 3.9° in OprN, respectively. In OprN, the inclination of H3 helix resulted from coiled-coil interactions between H3 and H8 helices (Figure 3.13B). Hydrogen bonds among Asn173, Gln414, and Glu418 are formed at the stating point of inclination of H3 helix. These residues correspond to Thr181, Leu421, and Gln425 in OprM and Thr176, Ser417, and Glu421 in OprJ, suggesting that the disappearance of hydrogen bonds forms straight H3 helices of OprM and OprJ. Ser180 of OprN is conserved in OprM as Ser188 and in OprJ as Ser183, whereas coiled-coil interactions are different (Figure 3.13B and 3.13C). In OprN, Ser180 interacts with Glu411, and Arg398 is extruded from intraprotomer groove due to movement of H3 helix. In OprM, Ser188 interacts with Arg405 and Tyr411, but does not with Gln418, which corresponds to Glu411 of OprN. These interactions pull H3 helix toward the outer coiled-coil helices at the periplasmic end of α-barrel domain. In OprJ, Ser183 have no interaction with its around residues, forming the most straightest H3 helix. Thus, the H3 helix in the periplasmic end of the

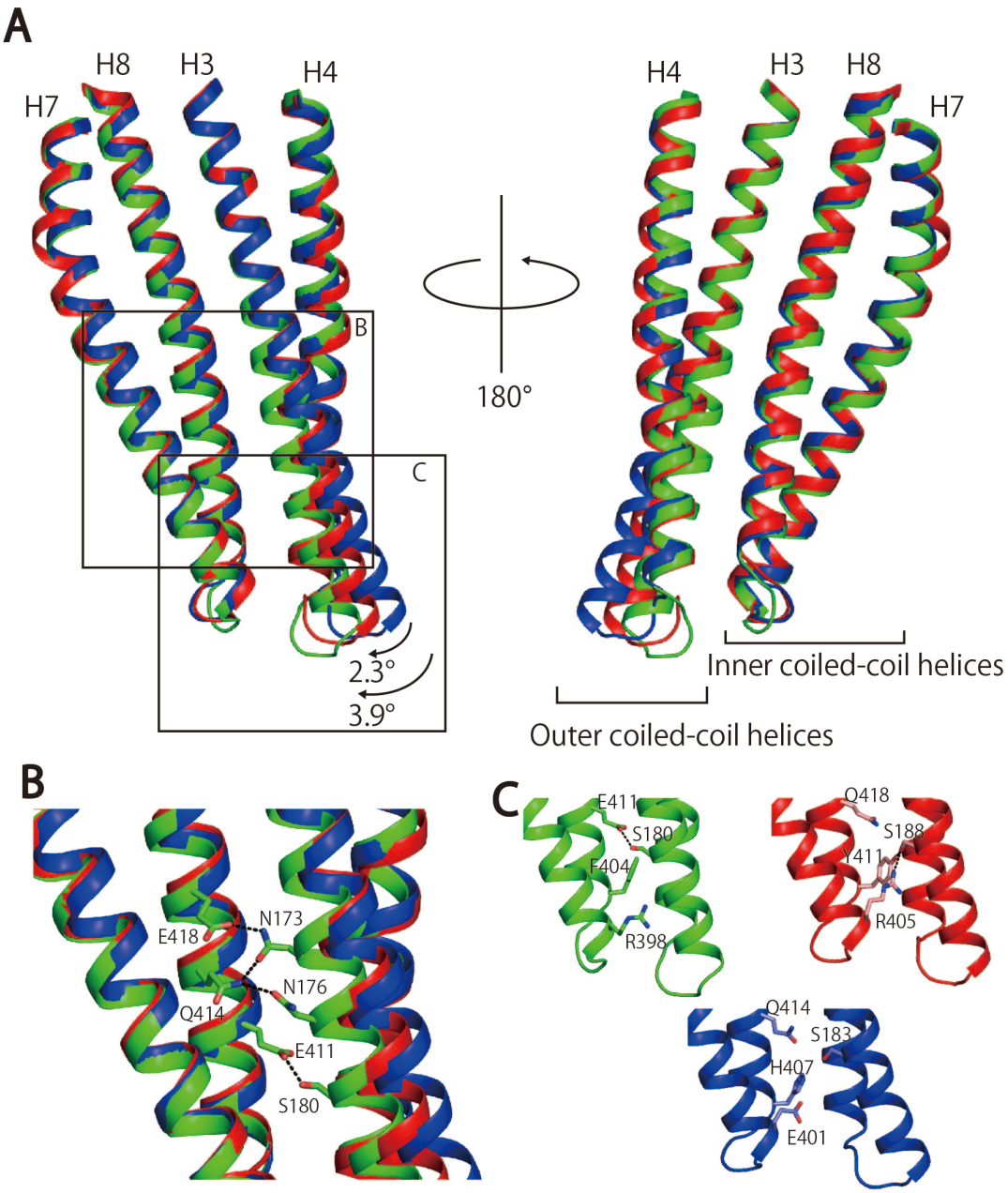

Figure 3.13 Superposition of OprN, OprJ, and OprM

(A) OprN, OprJ, and OprM are colored as in Figure 3.11. Residues of the outer and inner coiled-coil helices are Leu149–L230 and E361–L439 of OprN, Leu152–L233 and E364–L442 of OprJ, and L157–L238 and E368–L446 of OprM, respectively. (B) Close-up view of interactions between H3 and H8 helices of OprN. (C) Close-up view of the periplasmic ends of OprN, OprM, and OprJ.

α-barrel domain may adopt a unique structure in each OMF.

As a result of inclination of H3 helix, size of the periplasmic entrance also differs in OprN, OprJ, and OprM (Figure 3.14). In OprN, the distances between the oxygen atoms of Asp189, which is contained in H3 helix and lies at the outside of periplasmic entrance, are 38.7 Å, 39.2 Å, and 38.2 Å (Figure 3.14A). The corresponding distances between the oxygen atoms of Ala192 in OprJ and Asp197 in OprM are 44.6 Å, 42.9 Å, and 44.0 Å, and 40.6 Å, respectively (Figure 3.14B and 3.14C). In contrast, the distances between the oxygen atoms of Asp197 in OprN, Asp200 in OprJ, and Asp205 in OprM, which are contained in H4 helices and lie at the inside of periplasmic entrance, show similar values (Figure 3.14). Cross-linking experiments and cryoEM structure analysis showed that OMF interacts with MFP at the periplasmic end and entrance of α-barrel domain (Figure 1.5) (Lobedanz, S. *et al.* 2007; Du, D. *et al.* 2014), which correspond to the position where OprN, OprJ, and OprM differ in the structure of their H3 helices. Small and localized structural differences may be important for a binding and selectivity within each MFP. Furthermore, structural comparison of OprN, OprJ, and OprM suggest a possibility that a diameter of cylinder formed by α-hairpin domain of MFP may be different among each tripartite efflux pump.

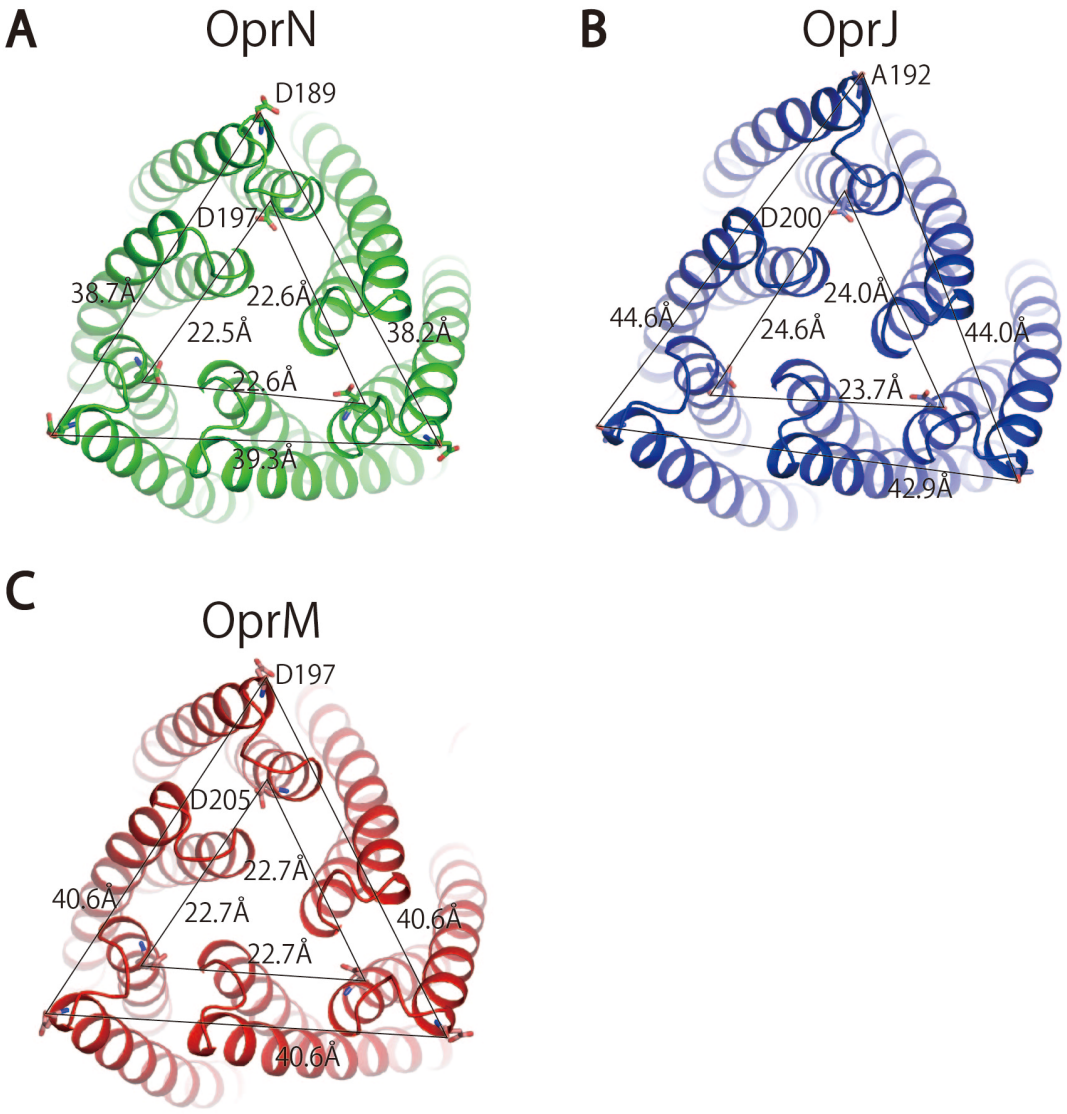

Figure 3.14 Comparison of the periplasmic entrance of OprN, OprJ, OprM

(A, B, C) OprN, OprJ, and OprM are colored in as Figure 3.11. Carbon atoms of OprN, OprJ, and OprM are colored in green, light blue, and light red, respectively. Oxygen and nitrogen atoms are colored in red and blue, respectively.

3.6 Electrostatic distribution of OprN, OprJ, and OprM

Figure 3.15A shows the internal electrostatic distributions of OprN, OprJ, and OprM, which have an almost negative character. Such negatively charged interiors are also observed in other solved OMFs, such as TolC and CusC (Kulathila, R. *et al.* 2011; Lei, H. T. *et al.* 2014). The distribution of negative charges may facilitate antibiotic extrusion. However, at the periplasmic end, where MFP interacts with OMF, the electrostatic distributions along interprotomer and intraprotomer grooves of OprN, OprJ, and OprM are different (Figure 3.15B). In the crystal structure of OprJ, although the overall structure is more similar to that of OprM than that of OprN, the electrostatic distributions within the interprotomer and intraprotomer grooves are more positive than those of the grooves in OprM. Residues such as Arg180, Arg190, Arg191, Lys394, Lys397, and Arg399 provide the positive charges in the grooves of OprJ. In the crystal structure of OprN, the interprotomer and intraprotomer grooves have more negatively electrostatic distributions than those of OprM, resulting from the presence of Glu175, Glu179, Glu185, Asp189, Glu195, Asp202, Glu384, Glu399, and Glu411. In the crystal structure of OprM, the periplasmic end has a balanced electrostatic distribution, suggesting that neutral charge may be important for forming the tripartite efflux pumps with a number of MFP-RND transporters. In addition to the charged residues, a number of solvent-exposed polar residues are located at the interprotomer and intraprotomer grooves of OprN, OprJ, and OprM. The polar and charged residues exhibit little similarity between these OMFs, but may be important for *in vivo* function of tripartite efflux pumps. Indeed, Janganan *et al.* showed that mutations of polar and charged residues at the interprotomer and intraprotomer grooves of MtrE have a detrimental effect on MtrCD-MtrE function (Janganan, T. K. *et al.* 2011). Based on the structural comparisons (Figure 3.11–3.14) and electrostatic distributions (Figure 3.15) of OprN, OprJ, and OprM, it is proposed that the overall structures of *P. aeruginosa* OMFs may

be optimized to maximize antibiotic transport activity by each tripartite efflux pump, and that the variety of polar and charged residues in the intraprotomer and interprotomer grooves may be important for their *in vivo* function.

OMF exchange experiments revealed that OprM is fully functional in complex with MexAB, MexCD, and MexEF, and OprJ is partially functional in complex with MexAB, whereas OprN is not (Yoneyama, H. *et al.* 1998; Maseda, H. *et al.* 2000). The electrostatic distribution of OprM at the interprotomer and intraprotomer grooves of periplasmic entrance of α-barrel domain is more similar to that of OprJ than that of OprN (Figure 3.15 C). This suggests that the electrostatic distribution at the periplasmic entrance regions may be important for formation of functional tripartite efflux pumps with MexAB.

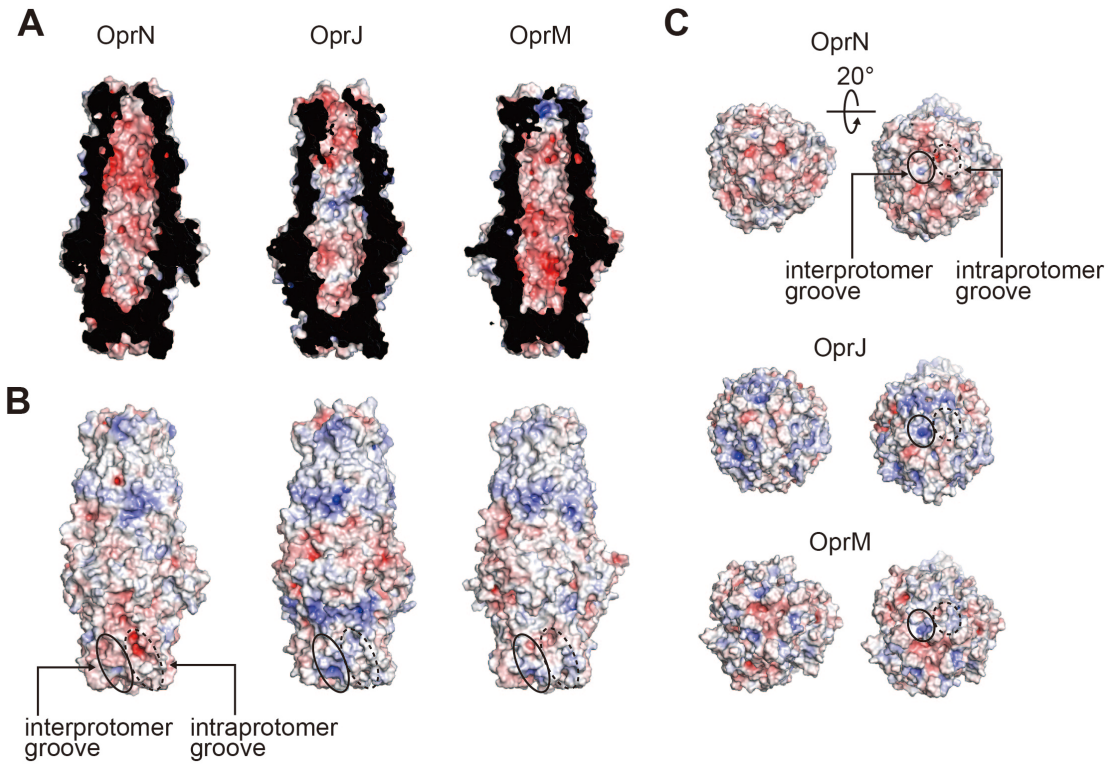

Figure 3.15 Electrostatic distributions OprN, OprJ, and OprM

Electrostatic distributions at inside (A), outside (B), and periplasmic entrance (C) are shown and colored by charge (red: negative -10 kT/e; blue : positive +10 kT/e).

3.7 Closed state at the β-barrel and α-barrel domain

The structural comparison indicated that the crystal structures of OprN, OprJ, and OprM may be optimized for each tripartite efflux pump and that they differ in their outer coiled-coil helices and electrostatic distribution at the periplasmic end and entrance of α-barrel domain. However, closed states of OprN, OprJ, and OprM are similar, forming a partially occluded pore at the β-barrel domain and a tightly sealed gate at the α-barrel domain (Figure 3.16). The closed state may be important for preventing an entry of antibiotics into bacterial cell.

The partially occluded pores in the β-barrel domain of OprN, OprJ, and OprM are formed a L1 loop. The L1 loop of OprN is shorter than those of OprJ and OprM, but the pore size is the smallest in OprN (Figure 3.16A). The pore diameters are 5–7 Å for

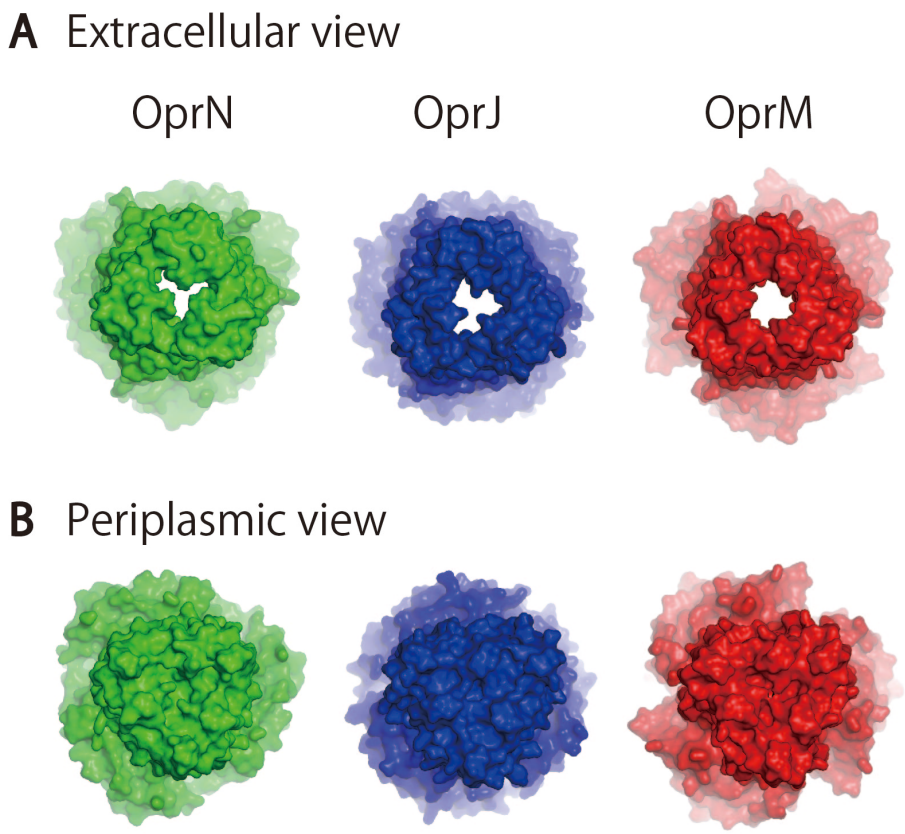

Figure 3.16 Surface views of OprN, OprJ, and OprM

Surface views from the extracellular side (A) and from the periplasmic side (B) of OprN, OprJ, and OprM.

OprN at Val98, 6–8 Å for OprJ at Ala100, and 6–8 Å for OprM at Thr105. In OprN, the L1 loop extends toward the center of the pore and is stabilized by interactions with Gln94–Ala313 and Glu100–Arg305 (Figure 3.17). These residues and interactions are not conserved in OprJ and OprM. In the crystal structure of OprN and OprJ, the partially occluded pore formed by the L1 loop is not enough to extrude antibiotics from interior space of OMF. The crystal structure of OprM showed large temperature factors for the extracellular loops and β-strands (Akama, H. *et al.* 2004), and the normal mode analysis of OprM proposed movements involving twist and extension to open the pore (Phan, G. *et al.* 2010). In the crystal structures of OprN and OprJ, the extracellular loop and β-strands had high temperature factors. Hence, the movements that open the pore may be similar in OprN and OprJ.

At the periplasmic end of the α-barrel domain, entrances to the internal cavity of OprN

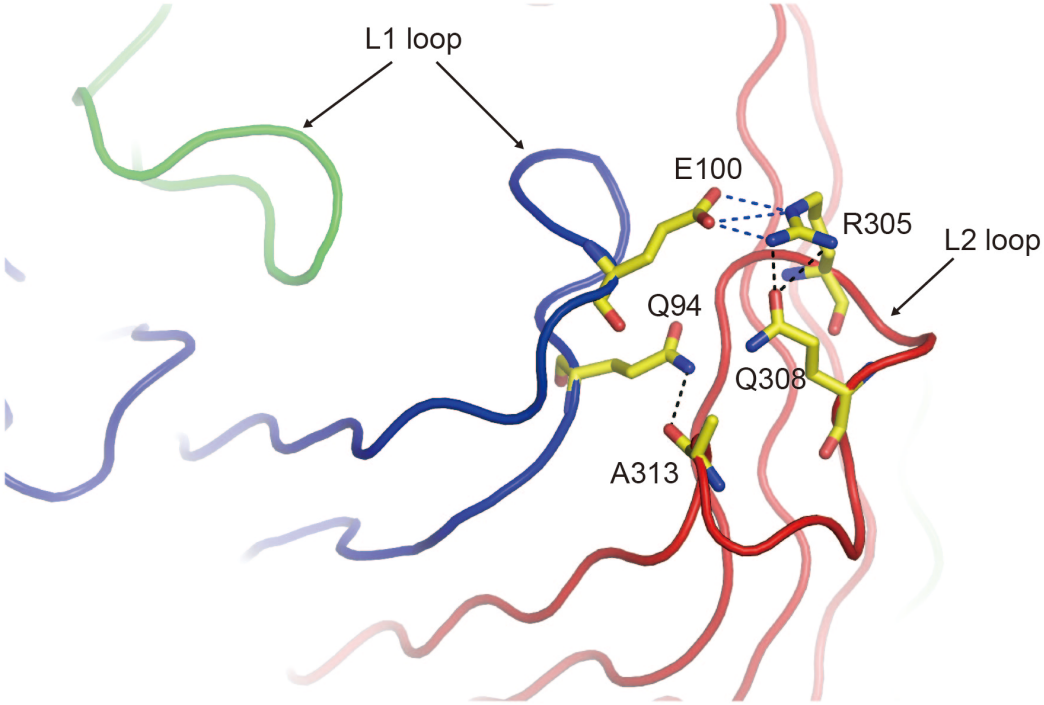

Figure 3.17 Interactions at the extracellular loop of OprN

Atoms and interactions are colored as in Figure 3.8 and Figure 3.10, respectively.

and OprJ are tightly sealed, and antibiotics cannot be extruded into the extracellular space. Like OprM, the periplasmic gates of OprN and OprJ are formed by a hydrophilic layer, hydrophobic interactions between Leu of each protomer, and a salt bridge between Asp of one protomer and Arg of the following protomer (Figure 3.18). The hydrophobic Leu ring is inserted into a space between the hydrophilic layer and the salt bridge (Figure 3.19). Two water molecules located at the inside and outside of Leu ring of OprN (Figure 3.19). Thus, the hydrophobic Leu ring may not allow the entry of even a water molecule. In the periplasmic gate, residues forming the hydrophobic interaction and salt bridge are conserved in OprN, OprJ, and OprM. In contrast, the hydrophilic layer of OprN shows a variety: Asp403 in OprN, Asn406 in OprJ, and Asn410 in OprM. These results suggest that hydrophobic Leu ring and salt bridge between Asp and Arg may be the conserved motif stabilizing the periplasmic gate in *P. aeruginosa* OMF. The narrowest points of the periplasmic gates are 4.0 Å at Leu405 in OprN and 3.4 Å at Leu408 in OprJ, which are measured between the side chain carbon ($C^{\delta 2}$) atoms of Leu. The tightly sealed periplasmic gate must be opened to allow the antibiotics entry.

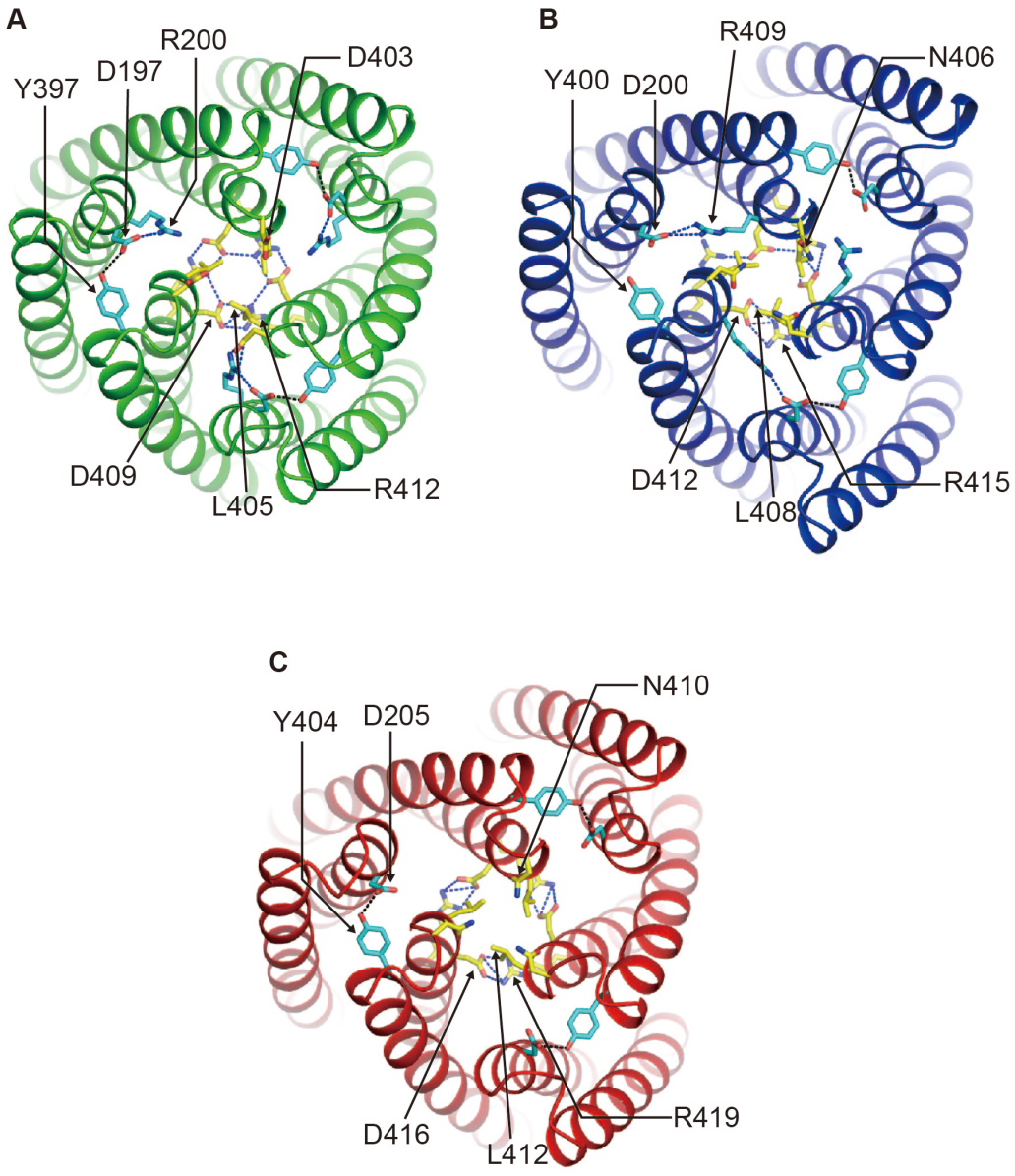

Figure 3.18 Interactions at the periplasmic gate of OprN, OprJ, and OprM

(A, B, C) The periplasmic gates of OprN (A), OprJ (B), and OprM (C) are shown as green, blue, and red, respectively. Carbon atoms of the periplasmic gate and the intraprotomer and interprotomer network are colored in yellow and cyan, respectively. Nitrogen and oxygen atoms are colored in blue and red, respectively. Interactions are colored as in Figure 3.10.

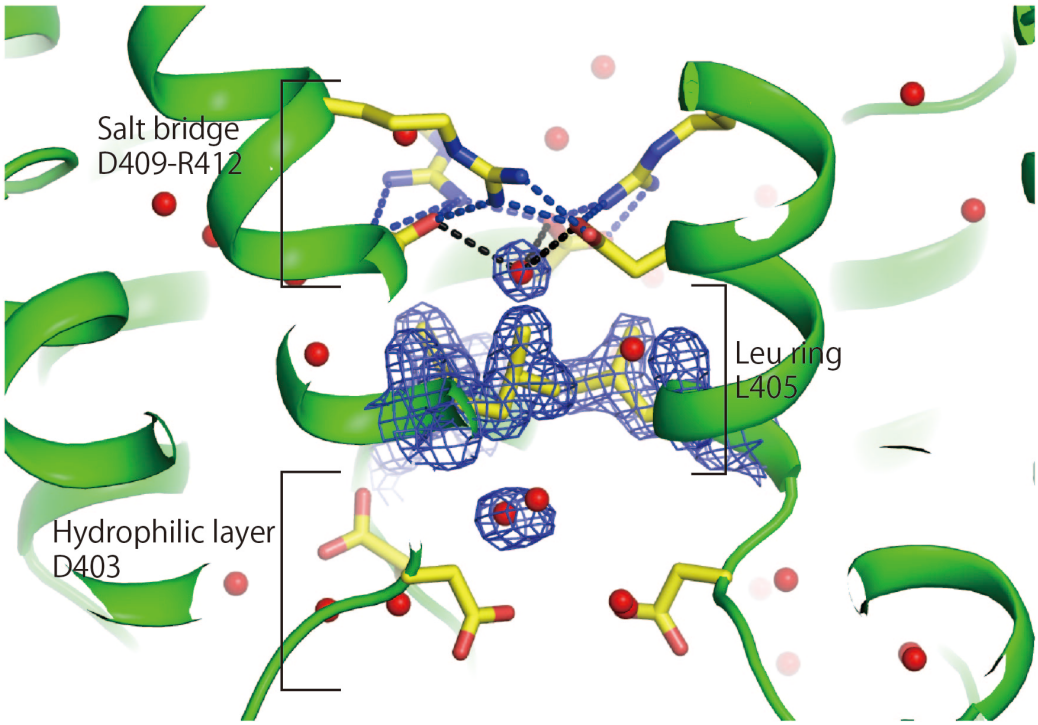

Figure 3.19 Periplasmic gate of OprN

Atoms are colored as in Figure 3.8. $2m|F_o|$-$D|F_c|$ electron density of Leu405 and two water molecules are contoured at 1.5 σ. Interactions are colored as in Figure 3.10.

3.8 Opening of the periplasmic gate of α-barrel domain

Du *et al.* showed that a binding of MFP to OMF leads to the opening of the periplasmic gate (Du, D. *et al.* 2014). In addition, crystallization conditions or the mutation of residues forming interprotomer and intraprotomer interactions at the periplasmic end are able to induce the opening of the periplasmic gate (Lei, H. T. *et al.* 2014; Bavro, V. N. *et al.* 2008; Pei, X. Y. *et al.* 2011). The crystal structure of MtrE showed an open state without mutations (Lei, H. T. *et al.* 2014), and the residues forming the hydrophobic Leu ring and salt brigde are conserved: Leus401, Asp405, and Arg408.

Superposing the OprN and MtrE structure revealed that the position of the α-barrel domain is similar but there are large outward rearrangements of coiled-coil helices at the periplasmic entrance (Figure 3.20A). In particular, the rearrangement of the inner coiled-coil helices, which contain the hydrophobic Leu ring and salt bridge, may be important for opening the periplasmic gate, resulting in increment of the pore size at the periplasmic entrance. In OprN, the distances between the oxygen atoms of Gly400, which is a conserved residue and lie on the periplasmic tip, are 15.3 Å, 16.6 Å, and 18.5 Å (Figure 3.20B). In MtrE, the corresponding distances between the oxygen atoms of Gly396 are 25.9 Å (Figure 3.20B). By comparing OprJ and MtrE, and OprM and MtrE, it is also revealed that the inner coiled-coils of OprJ and OprM may move in order to open the periplasmic gate (Figure 3.20C, D, E, and F). In the outer coiled-coil helices, the positions of H4 are similar, whereas those of H3 are different (Figure 3.21). As noted above, the H3 helices adopt unique structures in OprN, OprJ, and OprM (Figure 3.13). Furthermore, X-ray crystallographic studies of TolC revealed that the outer coiled-coil helices move outward, whereas the periplasmic tips of the inner coiled-coil helices maintain the same positions (Bavro, V. N. *et al*. 2008; Pei, X. Y. *et al.* 2011). These observations suggest that opening and closing of the periplasmic gate may be

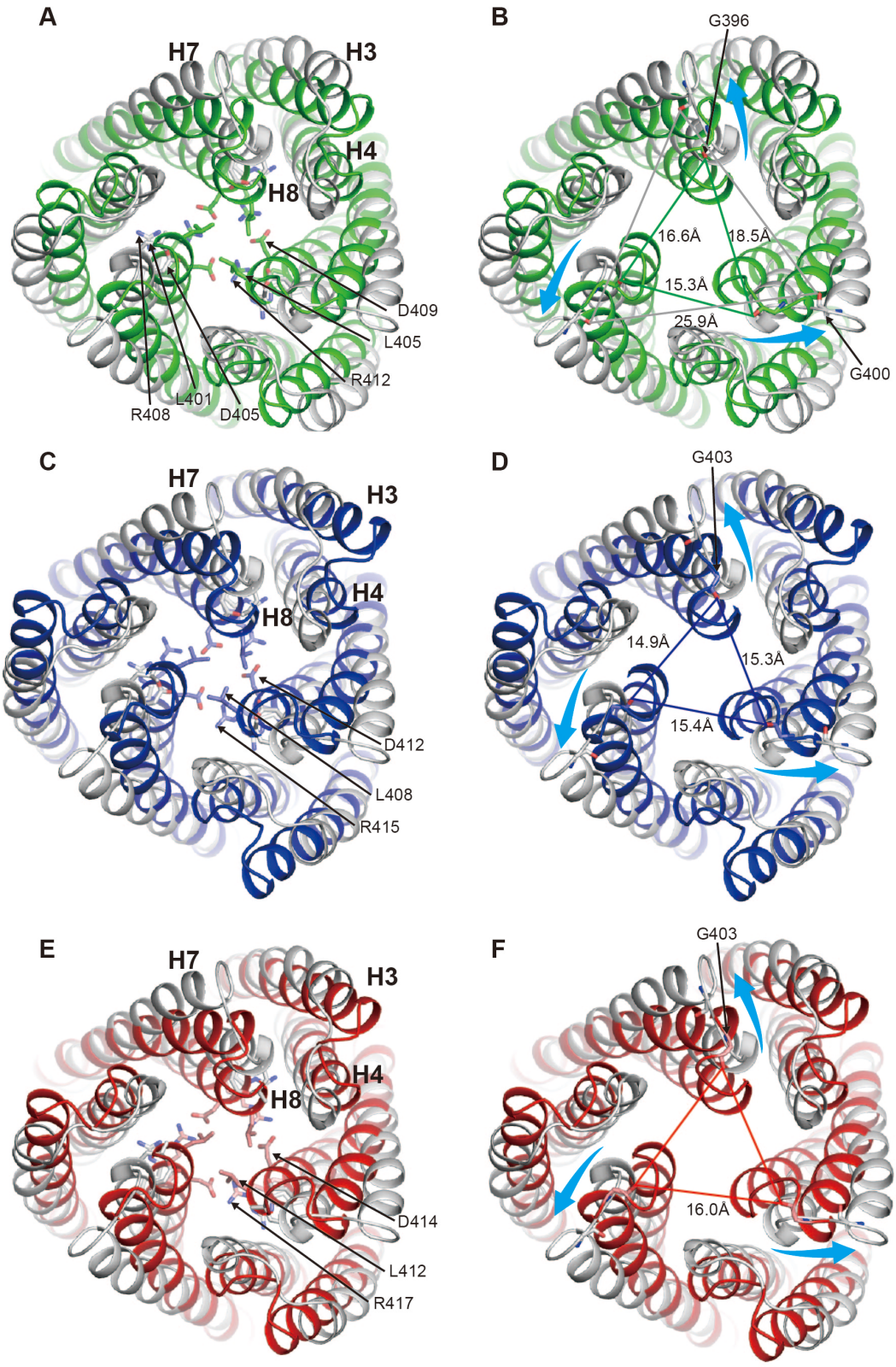
A
H7
H3
H4
H8
D409
L405
R412
L401
D405
R408
B
G396
16.6Å
18.5Å
15.3Å
25.9Å
G400
C
H7
H3
H4
H8
D412
L408
R415
D
G403
14.9Å
15.3Å
15.4Å
E
H7
H3
H4
H8
D414
L412
R417
F
G403
16.0Å

Figure 3.20 Comparison of the periplasmic entrance of OprN, OprJ, OprM, and MtrE

(A, B, C, D, E, F) Superposition of OprN, OprJ, OprM, and MtrE (PDB ID: 4MT0). OprN, OprJ, OprM, and MtrE are colored in green, blue, red, and gray, respectively. Conserved residues forming the periplasmic gate and Gly at the periplasmic tip are shown as a stick model. Carbon atoms of OprN, OprJ, OprM, and MtrE are colored in green, light blue, light red, and gray, respectively. Nitrogen and oxygen atoms are colored in blue and red, respectively.

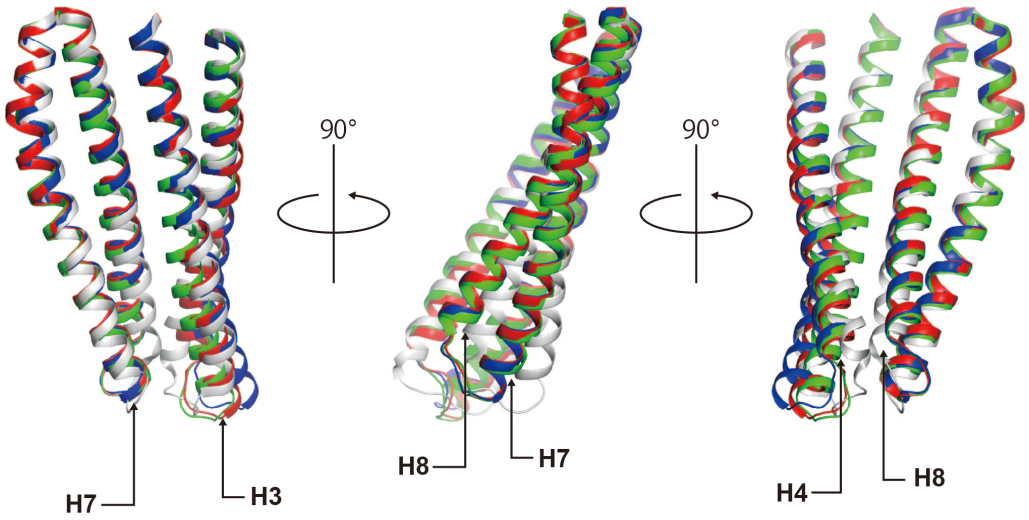

Figure 3.20 Comparison of the coiled-coil helices of OprN, OprJ, OprM, and MtrE

OprN, OprJ, OprM, and MtrE are colored as in Figure 3.19. Residues of the outer and inner coiled-coil helices are Leu149–L230 and E361–L439 of OprN, Leu152–L233 and E364–L442 of OprJ, L157–L238 and E368–L446 of OprM, and L145–L226 and D357–L435 of MtrE, respectively.

regulated by rearrangement of the inner coiled-coil helices, and that the outer coiled-coil helices may be fixed at unique positions in each OMF and function as pillars during the movement of the inner coiled-coil helices.

The closed state is maintained by the interprotomer and intraprotomer interactions at the periplasmic end of α-barrel domain. In TolC, the interprotomer interaction is formed by Thr152–Arg367 and Asp153–Arg367, while Asp153 interacts with Tyr362 and forms the intraprotomer interaction (Koronakis, V. *et al.* 2000). Disrupting these interactions increase the pore size at the periplasmic tip (Bavro, V. N. *et al*. 2008; Pei, X. Y. *et al.* 2011). Asp153–Tyr362 forms the most important interaction, and it is considered that the binding of AcrA to TolC may disrupt this interaction (Pei, X. Y. *et al.* 2011). The intraprotomer interactions are conserved as Asp197 and Tyr397 in OprN, Asp200 and Tyr400 in OprJ, and Asp205 and Tyr404 OprM, respectively (Figure 3.18). In the crystal structure of OprN, there are some additional intraprotomer interactions, which are formed by Arg200 and Asp403, at the periplasmic end of the α-barrel domain (Figure 3.18A). The interaction between Asp403 and Arg200 is observed at only one protomer. Asp403 is the residue that forms the hydrophilic layer of periplasmic gate; the movement of Asp403 in the H7–H8 loop causes its interaction with Arg200. In contrast, Arg200 of all protomer form a salt bridge with Asp197. These results indicate that the intraprotomer interactions between Arg197, Arg200, and Tyr397 are the most important interactions at the periplasmic end of α-barrel domain.

In the crystal structure of OprJ, Arg409, which is not conserved in OprN and OprM, locates at a near position of Asp200, and may form interprotomer interaction (Figure 3.18B). As in TolC, the crystal structures of OprN, OprJ, and OprM suggest that the intraprotomer interaction is the most critical for maintaining the closed state.

Chapter 4
Conclusion

Tripartite efflux pumps extrude functionally and structurally dissimilar antibiotics from bacterial cell. MexAB-OprM, MexCD-OprJ, MexEF-OprN, and MexXY-OprM are the main tripartite efflux pumps responsible for multidrug resistance in *P. aeruginosa*. The outer membrane factors, OprM, OprJ, and OprN, are essential components for tripartite efflux pump function. Structural information is therefore important for understanding the basis for multidrug resistance of *P. aeruginosa.* However, structures of OprJ and OprN have not been determined. In this study, we have determined the crystal structures of OprN(*P*321), OprN(*I*4), and OprJ at resolutions of 2.70 Å, 1.69 Å, and 3.10 Å, respectively.

Since the crystal structure of OprN(*I*4) was determined at 1.69 Å resolution, it was revealed that the N-terminal cysteine was triacylated by N-acyl and S-diaclyglycerol functional groups (Figure 3.7). Furthermore, in the border region between the α-barrel and β-barrel domains, detail interactions with water and detergent molecules were determined (Figure 3.8–3.10). These structures showed a state of OprN anchoring the outer membrane.

The overall structures of OprN and OprJ were similar to that of OprM. However, structural comparison of OprN, OprJ, and OprM revealed structural differences of the equatorial domain and the H3 helices at the periplasmic end and entrance of α-barrel domain (Figure 3.11–3.14). In contrast to large structural differences of the equatorial domain, those of H3 helices were small and local. At periplasmic end of α-barrel domain, electrostatic distributions along the interprotomer and intraprotomer grooves of OprN, OprJ, and OprM were also different (Figure 3.15). The periplasmic end of α-barrel domain corresponds to the position where OMF binds to MFP. Thus, it is

proposed that structures of *P. aeruginosa* OMFs may be optimized to maximize antibiotic transport activity by each tripartite efflux pump, and that localized structural difference of H3 helices may be important for a binding and selectivity within each MFP.

On the other hand, the tightly sealed gate at the periplasmic end of α-barrel domain was common among OprN, OprJ, and OprM. The periplasmic gate consisted of hydrophilic layer, hydrophobic interaction, and hydrophilic interaction. Among these structural features, residues forming hydrophobic and hydrophilic interactions are conserved in OprN, OprJ, and OprM. Moreover, the intraprotomer interaction fixing the closed periplasmic gate is also conserved. These results suggested that the structure and residues maintaining the closed state are important for *P. aeruginosa* OMFs.

The understanding for the structural character of OprN and OprJ is acquired, and findings in this study suggest that *P. aeruginosa* OMFs are optimized for a particular MFP. In the future, X-ray crystallography of the OMF-MFP complex and mutagenesis experiments will help elucidate the basis of recognition between OMF and MFP in *P. aeruginosa*.

Reference

Adams, P. D., Afonine, P. V., Bunkóczi, G., Chen, V. B., Davis, I. W., Echols, N., Headd, J. J., Hung, L. W., Kapral, G. J., Grosse-Kunstleve, R. W., McCoy, A. J., Moriarty, N. W., Oeffner, R., Read, R. J., Richardson, D. C., Richardson, J. S., Terwilliger, T. C., Zwart, P. H. *PHENIX*: a comprehensive Python-based system for macromolecular structure solution. *Acta. Crystallogr. D Biol. Crystallogr.* **66**, 213-221 (2010).

Akama, H., Kanemaki, M., Yoshimura, M., Tsukihara, T., Kashiwagi, T., Yoneyama, H., Narita, S., Nakagawa, A., Nakae, T. Crystal Structure of the Drug Discharge Outer Membrane Protein, OprM, of *Pseudomonas aeruginosa*. DUAL MODES OF MEMBRANE ANCHORING AND OCCLUDED CAVITY END *J. Biol. Chem.* **279**, 52816-52819 (2004).

Akama, H., Matsuura, T., Kashiwagi, S., Yoneyama, H., Narita, S., Tsukihara T., Nakagawa, A., Nakae, T. Crystal Structure of the Membrane Fusion Protein, MexA, of the Multidrug Transporter in *Pseudomonas aeruginosa*. *J. Biol. Chem.* **279**, 25939-25942 (2004).

Bai, J., Bhagavathi, R., Tran, P., Muzzarelli, K., Wang, D., Fralick J. A. Evidence that the C-terminal region is involved in the stability and functionality of OprM in *E. coli*. *Microbiol. Res.* **169**, 425-431 (2014).

Baker, N. A., Sept, D., Joseph, S., Holst, M. J., McCammon, J. A. Electrostatics of nanosystems: application to microtubules and the ribosome. *Proc. Natl. Acad. Sci. USA*

98, 10037-10041 (2001).

Bavro, V. N., Pietras, Z., Furnham, N., Pérez-Cano, L., Fernández-Recio, J., Pei, X. Y., Misra, R., Luisi, B. Assembly and Channel Opening in a Bacterial Drug Efflux Machine. *Mol. Cell* **30**, 114-121 (2008).

Chuanchuen, R., Murata, T., Gotoh N., Schweizer H. P. Substrate-Dependent Untilization of OprM or OpmH by the *Pseudomonas aeruginosa* MexJK Efflux Pump. *Antimicrob. Agents Chemother.* **49**, 2133-2136 (2005).

Chuanchuen, R., Narasaki, C. T., Schweizer, H. P. The MexJK Efflux Pump of *Pseudomonas aeruginosa* Requires OprM for Antibiotic Efflux but Not for Efflux of Triclosan. *J. Bacteriol.* **184**, 5036-5044 (2002).

Colmer, J. A., Frallck J. A., Hamood, A. N. Isolation and characterization of a putative multidrug resistance pump form *Vibrio cholerae*. *Mol. Microbiol.* **27**, 63-72 (1998).

DeLano, W. L. The PyMOL molecular graphics system. DeLano Scientific, Palo Alto, CA, (2002).

Du, D., Wang, Z., James, N. R., Voss, J. E., Klimont, E., Ohene-Agyei, T., Venter, H., Chiu, W., Luisi, B. F. Structure of the AcrAB-TolC multidrug efflux pump. *Nature* **509**, 512-515 (2014).

Eda, S., Maseda, H., Yoshihara, E., Nakae, T. Assignment of the outer-membrane-subunit-selective domain of the membrane fusion protein in the tripartite xenobiotic efflux pump of *Pseudomonas aeruginosa*. *FEMS Microbiol. Lett.*

254, 101-107 (2006).

Eicher, T., Cha, H., Seeger, M. A., Brandstätter, L., El-Delik, J., Bohnert, J. A., Kern, W. V., Verrey, F., Grütter, M. G., Diederichs, K., Pos K. M. Transport of drugs by the multidrug transporter AcrB involves an access and a deep binding pocket that are separated by a switch-loop. *Proc. Natl. Acad. Sci. USA* **109**, 5687-5692 (2012).

Emsley, P., Lohkamp, B., Scott, W. G., Cowtan, K. Features and development of *Coot*. *Acta. Crystallogr. D Biol. Crystallogr.* **66**, 486-501 (2010).

Federici, L., Du, D., Walas, F., Matsumura, H., Fernandez-Recio, J., McKeegan, K. S., Borges-Walmsley, M. I., Luisi, B. F., Walmsley, A. R. The Crystal Structure of the Outer Membrane Protein VceC from the Bacterial Pathogen *Vibrio cholerae* at 1.8 Å Resolution. *J. Biol. Chem.* **280**, 15307-15314 (2005).

Fukuda, H., Hosaka, M., Hirai, K., Iyobe, S. New Norfloxacin Resistance Gene in *Pseudomonas aeruginosa* PAO. *Antimicrob. Agents Chemother.* **34**, 1757-1761 (1990).

Gotoh, N., Tsujimoto, H., Nomura, A., Okamoto, K., Tsuda, M., Nishino, T. Functional replacement of OprJ by OprM in the MexCD-OprJ multidrug efflux system of *Pseudomonas aeruginosa*. *FEMS Microbiol. Lett.* **165**, 21-27 (1998).

Gotoh, N., Tsujimoto, H., Tsuda, M., Okamoto, K., Nomura, A., Wada, T., Nakahashi, M., Nishino, T. Characterization of the MexC-MexD-OprJ Multidrug Efflux System in ΔmexA-mexB-OprM Mutants of *Pseudomonas aeruginosa*. *Antimicrob. Agents Chemother.* **42**, 1938-1943 (1998).

Guan, L., Nakae, T. Identification of Essential Charged Residues in Transmembrane Segments of the Multidrug Transporter MexB of *Pseudomonas aeruginosa*. *J. Bacteriol.* **183**, 1734-1739 (2001).

Janganan, T. K., Zhang, L., Bavro, V. N., Matak-Vinkovic, D., Barrera, P., Burton, M. F., Steel, P. G., Robinson, C. V., Borges-Walmsley, M. I., Walmsley, A. R. Opening of the Outer Membrane Protein Channel in Tripartite Efflux Pumps Is Induced by Interaction with the Membrane Fusion Partner. *J. Biol. Chem.* **286**, 5484-5493 (2011).

Koronakis, V., Sharff, A., Koronakis, E., Luisi, B., Hughes, C. Crystal structure of the bacterial membrane protein TolC central to multidrug efflux and protein export. *Nature* **405**, 914-919 (2000).

Köhler, T., Michéa-Hamzehpour, M., Henze, U., Gotoh, N., Curty, L. K., Pechère, J. C. Characterization of MexE-MexF-OprN, a positively regulated multidrug efflux system of *Pseudomonas aeruginosa*. *Mol. Microbiol.* **23**, 345-354 (1997).

Krissinel, E., Henrick, K. Secondary-structure matching (SSM), a new tool for fast protein structure alignment in three dimensions. *Acta. Crystallogr. D Biol. Crystallogr.* **60**, 2256-2268 (2004).

Kulathila, R., Kulathila, R., Indic, M., van der Berg, B. Crystal Structure of *Escherichia coli* CusC, the Outer Membrane Component of a Heavy Metal Efflux Pump. *PLoS One* **6**, e15610 (2011).

Lei, H. T., Bolla, J. R., Bishop, N. R., Su, C. C., Yu, E. W. Crystal Structures of CusC Review Conformational Changes Accompanying Folding and Transmembrane Channel Formation. *J. Mol. Biol.* **426**, 403-411 (2014).

Lei, H. T., Chou, T. H., Su, C. C., Bolla, J. R., Kumar, N., Radhakrishnan, A., Long, F., Delmar, J. A., Do, S. V., Rajashankar, K. R., Shafer, W. M., Yu, E. W. Crystal Structure of the Open State of the *Neisseria gonorrhoeae* MtrE Outer Membrane Channel. *PLoS One* **9**, e97475 (2014).

Lei, Y., Sato, K., Nakae, T. Ofloxacin-resistant *Pseudomonas aeruginosa* mutants with elevated drug extrusion across the inner membrane. *Biochem. Biophys. Res. Commun.* **178**, 1043-1048 (1991).

Li, X. Z., Nikaido, H., Poole, K. Role of MexA-MexB-OprM in Antibiotic Efflux in *Pseudomonas aeruginosa*. *Antimicrob. Agents Chemother*. **39**, 1948-1953 (1995).

Li, X. Z., Poole, K. Mutational Analysis of the OprM Outer Membrane Component of the MexA-MexB-OprM Multidrug Efflux System of *Pseudomonas aeruginosa*. *J. Bacteriol.* **183**, 12-27 (2001).

Li, Y., Mima, T., Komori, Y., Morita, Y., Kuroda, T., Mizushima, T., Tsuchiya, T. A new member of the tripartite multidrug efflux pumps, MexVW-OprM, in *Pseudomonas aeruginosa*. *J. Antimicrob. Chemother.* **52**, 572-575 (2003).

Lobedanz, S., Bokma, E., Symmons, M. F., Koronakis, E., Hughes, C., Koronakis, V. A periplasmic coiled-coil interface underlying TolC recruitment and the assembly of bacterial drug efflux pumps. *Proc. Natl. Acad. Sci. USA* **104**, 4612-4617 (2007).

Lovell, S. C., Davis, I. W., Arendall, W. B. 3rd, de Bakker, P. I., Word, J. M., Prisant, M. G., Richardson, J. S., Richardson, D. C. Structure validation by Calpha geometry: phi,psi and Cbeta deviation. *Proteins* **50**, 437-450 (2003).

Maseda, H., Saito, K., Nakajima, A., Nakae, T. Variation of the *mexT* gene, a regulator of the MexEF-OprN efflux pump expression in wild-type strains of *Pseudomonas aeruginosa*. *FEMS Microbiol. Lett.* **192**, 107-112 (2000).

Maseda, H., Yoneyama, H., Nakae, T. Assignment of the Substrate-Selective Subunits of the MexEF-OprN Multidrug Efflux Pump of *Pseudomonas aeruginosa*. *Antimicrob. Agents Chemother.* **44**, 658-64 (2000).

Matsuo, Y., Eda, S., Gotoh, N., Yoshihara, E., Nakae, T. MexZ-mediated regulation of *mexXY* multidrug efflux pump expression in *Pseudomonas aeruginosa* by binding on the *mexZ-mexX* intergenic DNA. *FEMS Microbiol. Lett.* **238**, 23-28 (2004).

Mikolosko, J., Bobyk, K., Zgurskaya, H. I., Ghosh, P. Conformational Flexibility in the Multidrug Efflux System Protein AcrA. *Structure* **14**, 577-587 (2006).

Mima, T., Joshi, S., Gomez-Escalada, M., Schweizer, H. P. Identification and Characterization of TriABC-OpmH, a Triclosan Efflux Pump of *Pseudomonas aeruginosa* Requiring Two Membrane Fusion Proteins. *J. Bacteriol.* **189**, 7600-7609 (2007).

Mima, T., Kohira, N., Li, Y., Sekiya, H., Ogawa W., Kuroda, T., Tsuchiya, T. Gene cloning and characteristics of the RND-type multidrug efflux pump MuxABC-OpmB possessing two RND components in *Pseudomonas aeruginosa*. *Microbiology* **155**, 3509-3517 (2009).

Mima, T., Sekiya, H., Mizushima, T., Kuroda, T., Tsuchiya, T. Gene Cloning and Properties of the RND-Type Multidrug Efflux Pumps MexPQ-OpmE and MexMN-OprM from *Pseudomonas aeruginosa*. *Microbiol. Immunol.* **49**, 999-1002 (2005).

Mine, T., Morita, Y., Kataoka, A., Mizushima, T., Tsuchiya, T. Expression in *Escherichia coli* of a New Multidrug Efflux Pump, MexXY, from *Pseudomonas aeruginosa*. *Antimicrob. Agents Chemother.* **43**, 415-417 (1999).

Monlezun, L., Phan, G., Benabdelhak, H., Lascombe, M. B., Enguéné, V. Y., Picard, M., Broutin, I. New OprM structure highlighting the nature of the N-teminal anchor. *Front Microbiol.* 6, 667 (2015).

Morshed, S. R., Lei, Y., Yoneyama, H., Nakae, T. Expression of genes associated with antibiotic extrusion in *Pseudomonas aeruginosa*. *Biochem. Biophys. Res. Commun*. **210**, 356-362 (1995).

Murakami, S., Nakashima, R., Yamashita, E., Matsumoto, T., Yamaguchi, A. Crystal structures of a multidrug transporter reveal a functionally rotating mechanism. *Nature* **443**, 173-179 (2006).

Murata, T., Gotoh, N., Nishino, T. Characterization of outer membrane efflux proteins

OpmE, OpmD and OpmB of *Pseudomonas aeruginosa*: molecular cloning and development of specific antisera. *FEMS Microbiol. Lett.* **217**, 57-63 (2002).

Murshudov, G. N., Skubák, P., Lebedev, A. A., Pannu, N. S., Steiner, R. A., Nicholls, R. A., Winn, M. D., Long, F., Vagin, A. A. *REFMAC*5 for the refinement of macromolecular crystal structures. *Acta. Crystallogr. D. Biol. Crystallogr*. **7**, 355-367 (2011).

Nakae, T. Role of Membrane Permeability in Determining Antibiotic Resistance in *Pseudomonas aeruginosa*. *Microbiol. Immunol.* **39**, 221-229 (1995).

Nakajima, A., Sugimoto, Y., Yoneyama, H., Nakae, T. Localization of the Outer Membrane Subunit OprM of Resistance-Nodulation-Cell Division Family Multicomponent Efflux Pump in *Pseudomonas aeruginosa*. *J. Biol. Chem.* **275**, 30064-30068 (2000).

Nakashima, R., Sakurai, K., Yamasaki, S., Hayashi, K., Nagata, C., Hoshino, K., Onodera, Y., Nishino, K., Yamaguchi, A. Structural basis for the inhibition of bacterial multidrug exporters. *Nature* **500**, 102-106 (2013).

Nehme, D., Poole, K. Assembly of the MexAB-OprM Multidrug Pump of *Pseudomonas aeruginosa*: Component Interactions Defined by the Study of Pump Mutant Suppressors. *J. Bacteriol.* **189**, 6118-6127 (2007).

Nikaido, H. Prevention of Drug Access to Bacterial Targets: Permeability Barriers and Active Efflux. *Science* **264**, 382-288 (1994).

Okuda, S., Tokuda, H. Lipoprotein Sorting in Bacteria. *Annu. Rev. Microbiol.* **65**, 239-259 (2011).

Otwinowski, Z., Minor, W. Processing of X-ray Diffraction Data Collected in Oscillation Mode. *Method Enzymol.* **276**, 307-326 (1997).

Pei, X. Y., Hinchliffe, P., Symmons, M. F., Koronakis, E., Benz, R., Hughes, C., Koronakis, V. Structures of sequential open states in a symmetrical opening transition of the TolC exit duct. *Proc Natl Acad Sci USA* **108**, 2112-2117 (2011).

Pettersen, E. F., Goddard, T. D., Huang, C. C., Couch, G. S., Greenblatt, D. M., Meng, E. C., Ferrin, T. E. UCSF Chimera–a visualization system for exploratory research and analysis. *J. Comput. Chem.* **25**, 1605-1612 (2004).

Phan, G., Benabdelhak, H., Lascombe, M. B., Benas, P., Rety, S., Picard, M., Ducruix, A., Etchebest, C., Broutin, I. Structural and Dynamical Insights into the Opening Mechanism of *P. aeruginosa* OprM Channel. *Structure* **18**, 507-517 (2010).

Poole, K., Gotoh, N., Tsujimoto, H., Zhao, Q., Wada, A., Yamasaki, T., Neshat, S., Yamagishi, J., Li, X. Z., Nishino, T. Overexpression of the *mexC-mexD-oprJ* efflux operon in *nfxB*-type multidrug-resistant strains of *Pseudomonas aeruginosa*. *Mol. Microbiol.* **21**, 713-724 (1996).

Remans, K., Vercammen, K., Bodilis, J., Cornelis, P. Genome-wide analysis and literature-based survey of lipoproteins in *Pseudomonas aeruginosa*. *Microbiol.* **156**,

2597-2607 (2010).

Saito, K., Yoneyama, H., Nakae, T. *nalB*-type mutations causing the overexpression of the MexAB-OprM efflux pump are located in the *mexR* gene of the *Pseudomonas aeruginosa* chromosome. *FEMS Microbiol. Lett.* **179**, 67-72 (1999).

Sankaran, K., Wu, H. C. Lipid Modification of Bacterial Prolipoprotein. TRANSFER OF DIACYLGLYCERYL MOIETY FROM PHOSPHATIDYLGLYCEROL *J. Biol. Chem.* **269**, 19701-19706 (1994).

Schweizer, H. P. Efflux as a mechanism of resistance to antimicrobials in *Pseudomonas aeruginosa* and related bacteria: unanswered questions. *Genet. Mol. Res.* **2**, 48-62 (2003).

Seeger, M. A., Schiefner, A., Eicher, T., Verrey, F., Diederichs, K., Pos, K. M. Structural Asymmetry of AcrB Trimer Suggests a Peristaltic Pump Mechanism. *Science* **313**, 1295-1298 (2006).

Sekiya, H., Mima, T., Morita, Y., Kuroda, T., Mizushima, T., Tsuchiya, T. Functional Cloning and Characterization of a Multidrug Efflux Pump, MexHI-OpmD, from a *Pseudomonas aeruginosa* Mutant. *Antimicrob. Agents Chemother.* **47**, 2990-2992 (2003).

Sennhauser, G., Bukowska, M. A., Briand, C., Grütter, M. G. Crystal Structure of the Multidrug Exporter MexB from *Pseudomonas aeruginosa*. *J. Mol. Biol.* **389**, 134-145 (2009).

Shiba, T., Ishiguro, K., Takemoto, N., Koibuchi, H., Sugimoto, K. Purification and Characterization of the *Pseudomonas aeruginosa* NfxB Protein, the Negative Regulator of the *nfxB* Gene. *J. Bacteriol.* **177**, 5872-5877 (1995).

Su, C. C., Radhakrishnan, A., Kumar, N., Long, F., Bolla, J. R., Lei, H. T., Delmar, J. A., Do, S. V., Chou, T. H., Rajashankar, K. R., Zhang, Q., Yu, E. W. Crystal structure of the *Campylobacter jejuni* CmeC outer membrane channel. *Protein Sci.* **23**, 954-961 (2014).

Symmons, M. F., Bokma, E., Koronakis, E., Hughes, C., Koronakis V. The assembled structure of a complete tripartite bacterial multidrug efflux pump. *Proc. Natl. Acad. Sci. USA* **106**, 7173-7178 (2009).

Tamura, N., Murakami, S., Oyama, Y., Ishiguro, M., Yamaguchi, A. Direct Interaction of Multidrug Efflux Transporter AcrB and Outer Membrane Channel TolC Detected via Site-Directed Disulfide Cross-Linking. *Biochemistry* **44**, 11115-11121 (2005).

Vaguine, A. A., Richelle, J., Wodak, S. J. SFCHECK: a unified set of procedure for evaluating the quality of macromolecular structure-factor data and their agreement with atomic model. *Acta Crystallogr D Biol Crystallogr* **55**, 191-205 (1999).

Xu, Y., Lee, M., Moeller, A. Song, S., Yoon, B. Y., Kim, H. M., Jun, S. Y., Lee, K. Ha, N. C. Funnel-like Hexameric Assembly of the Periplasmic Adapter Protein in the Tripartite Multidrug Efflux Pump in Gram-negative Bacteria. *J. Biol. Chem.* **286**, 17910-17920 (2011).

Yamanaka, H., Morisada, N., Miyano, M., Tsuge, H., Shinoda, S., Takahashi, E., Okamoto, K. Amino-Acid Residues Involved in the Expression of the Activity of *Escherichia coli* TolC. *Microbiol. Immunol.* **48**, 713-722 (2004).

Yamanaka, H., Nomura, T., Morisada, N., Shinoda, S., Okamoto, K. Site-directed mutagenesis studies of the amino acid residue at position 412 of Escherichia coli TolC which is required for the activity. *Microb. Pathog*. **33**, 81-89 (2002).

Yoneyama, H., Maseda, H., Kamiguchi, H., Nakae, T. Function of the Membrane Fusion Protein, MexA, of the MexA, B-OprM Efflux Pump in *Pseudomonas aeruginosa* without an Anchoring Membrane. *J. Biol. Chem.* **275**, 4628-4634 (2000).

Yoneyama, H., Ocaktan, A., Gotoh, N., Nishino, T., Nakae, T. Subunit Swapping in the Mex-Extrusion Pumps in *Pseudomonas aeruginosa*. *Biochem. Biophys. Res. Commun.* **244**, 898-902 (1998).

Yoneyama, H., Ocaktan, A., Tsuda, M., Nakae, T. The Role of *mex*-Gene Products in Antibiotic Extrusion in *Pseudomonas aeruginosa*. *Biochem. Biophys. Res. Commun*. **233**, 611-618 (1997)

Vagin, A., Teplyakov, A. Molecular replacement with *MOLREP*. *Acta. Crystallogr. D Biol. Crystallogr.* **66**, 22-25 (2010).

Wadman, S. W., Sherman, D. R., Hickey, M. J., Coulter, S. N., Zhu, Y. Q., Warrener, P., Nguyen, L. Y., Shawar, R. M., Folger, K. R., Stover, C. K. Characterization of a

Pseudomonas aeruginosa Efflux Pump Contributing to Aminoglycoside Impermeability. *Antimicrob. Agents Chemother.* **43**, 2975-2983 (1999).

Wallace, A. C., Laskowski, R. A., Thornton, J. M. LIGPLOT: a program to generate schematic diagrams of protein-ligand interactions. *Protein Eng*. **8**, 127-134 (1996).

Winn, M. D., Ballard, C. C., Cowtan, K. D., Dodson, E. J., Emsley, P., Evans, P. R., Keegan, R. M., Krissinel, E. B., Leslie, A. G., McCoy, A., McNicholas, S. J., Murshudov, G. N., Pannu, N. S., Potterton, E. A., Powell, H. R., Read, R. J., Vagin, A., Wilson, K. S. Overview of the *CCP*4 suite and current developments. *Acta. Crystallogr. D Biol. Crystallogr.* **67**, 235-242 (2011).

List of publication

Yonehara, R., Yamashita, E., Nakagawa A. Crystal structures of OprN and OprJ, outer membrane factors of multidrug tripartite efflux pumps from *Pseudomonas aeruginosa*. *Proteins* (in press)